GÖTEBORG UNIVERSITY

Optical Excitation and Decay Dynamics of Fullerenes

MARTIN HEDÉN

Department of Physics
Göteborg University

Optical Excitation and Decay Dynamics of Fullerenes

Martin Hedén

Akademisk avhandling för avläggande av filosofie doktorsexamen i fysik vid Göteborgs universitet. Avhandlingen försvaras vid en offentlig disputation kl. 9:30 den 27:e maj 2005 i sal KC, Kemihuset, Chalmers tekniska högskola, Göteborg.

Fakultetsopponent: Professor Bernd Huber
CEA-CIRIL, Caen, Frankrike

Examinator: Professor Eleanor E. B. Campbell

Avhandlingen försvaras på engelska

Avhandlingen finns tillgänglig vid forskargruppen för Atomfysik, Institutionen för fysik, Göteborgs universitet.

Institutionen för fysik
GÖTEBORGS UNIVERSITET

Göteborg 2005

Optical Excitation and Decay Dynamics of Fullerenes

Martin Hedén
Department of Physics
Göteborg University
SE-41296 Göteborg, Sweden

Abstract

The dynamics of highly excited fullerenes have been studied experimentally. Attention has been paid to excitation processes, such as excitation of Rydberg states and excitation and lifetime of the triplet state in C_{60}. Both the latter processes where found to depend on the vibrational energy of C_{60}. The triplet lifetime decreases exponentially with increasing vibrational energy while excitation of Rydberg states requires a vibrational energy in the fullerene. Relaxation mechanisms were also investigated, in particular radiative cooling. For the large range of fullerenes measured the emissivity was measured to be $5{\cdot}10^{-4} - 15{\cdot}10^{-4}$. No difference in the radiation behaviour between empty fullerenes and fragments of the endohedral fullerene La@C_{82} was found. Moreover, clusters of fullerenes were observed to decay by fusion followed by sequential C_2 evaporation after femtosecond laser excitation.
In addition, the internal energy distribution obtained by molecules after multiphoton absorption from a laser was examined. For a realistic description of the laser and molecular beam the internal energy distribution is not well described by the commonly used Poisson distribution but rather follows a power law up to a cutoff proportional to the fluence.

Keywords: fullerenes, triplet state, radiative cooling, clusters of fullerenes, molecular fusion, Rydberg states, mass spectrometry, time of flight, endohedral fullerenes

Thesis for the degree of Doctor of Philosophy

Optical Excitation and Decay Dynamics of Fullerenes

Martin Hedén

Department of Physics
GÖTEBORG UNIVERSITY

Göteborg 2005

Optical Excitation and Decay Dynamics of Fullerenes
Martin Hedén
ISBN 91-628-6541-2

Atomfysik
Institutionen för fysik
Göteborgs universitet
SE-41296 Göteborg
Sweden
Tel: +46 (0)31-772 3256, Fax: +46 (0)31-772 3496

Chalmers reproservice
Göteborg 2005

Optical Excitation and Decay Dynamics of Fullerenes

Martin Hedén
Atomic Physics
Department of Physics
Göteborg University
SE–412 96 Göteborg, Sweden

Abstract

The dynamics of highly excited fullerenes have been studied experimentally. Attention has been paid to excitation processes, such as excitation of Rydberg states and excitation and lifetime of the triplet state in C_{60}. Both the latter processes where found to depend on the vibrational energy of C_{60}. The triplet lifetime decreases exponentially with increasing vibrational energy while excitation of Rydberg states requires a vibrational energy in the fullerene. Relaxation mechanisms were also investigated, in particular radiative cooling. For the large range of fullerenes measured the emissivity was measured to be $5{\cdot}10^{-4} - 15{\cdot}10^{-4}$. No difference in the radiation behaviour between empty fullerenes and fragments of the endohedral fullerene La@C_{82} was found. Moreover, clusters of fullerenes were observed to decay by fusion followed by sequential C_2 evaporation after femtosecond laser excitation.
In addition, the internal energy distribution obtained by molecules after multiphoton absorption from a laser was examined. For a realistic description of the laser and molecular beam the internal energy distribution is not well described by the commonly used Poisson distribution but rather follows a power law up to a cutoff proportional to the fluence.

Keywords: fullerenes, triplet state, radiative cooling, clusters of fullerenes, molecular fusion, Rydberg states, mass spectrometry, time of flight, endohedral fullerenes

Sammanfattning

Dynamiken hos högt exciterade fullerener i gasfas har studerats med experimentella metoder. Excitationsprocesser, såsom excitation av Rydbergstillstånd och excitation och livstid hos triplettillståndet i C_{60}, har ägnats särskild uppmärksamhet. Båda processerna fanns bero starkt på den interna vibrationsenergin hos C_{60}. Triplettillståndets livstid minskar exponentiellt med ökande vibrationsenergi medan excitation av Rydbergstillstånd kräver vibrationsenergi i fullerenen.
Vidare har även relaxationsmekanismer hos fullerener och kluster av fullerener undersökts. För fullerener har fokus legat på fotonemission och emissiviteten för fullerener av flera olika storlekar uppmättes till $5{\cdot}10^{-4} - 15{\cdot}10^{-4}$. Ingen skillnad i strålningsbeteendet mellan fullerener och fragment av den endohedrala fullerenen $La@C_{82}$ kunde detekteras. Kluster av fullerener visade sig fusionera för att sedan emittera C_2-molekyler efter att ha exciterats med femtosekundlaserpulser.
Dessutom har den interna energidistributionen hos molekyler efter multifotonabsorbtion med hjälp av laser studerats. För en realistisk beskrivning av både laser och molekylstråle så är den vanligt förekommade Poissondistributionen inte en bra representation av den interna energifördelningen hos molekylerna utan distributionen följer snarare en potenslag upp till en gräns där den klingar av. Gränsvärdet är proportionellt mot laserflödet.

Appended Papers

This thesis is partly based on work reported in the following papers, referred to by Roman numerals in the text:

I. M. Hedén, A. V. Bulgakov, K. Mehlig and E. E. B. Campbell, *J. Chem. Phys.* ***118****, 7161 (2003)*
Determination of the triplet state lifetime of vibrationally excited C_{60}

II. K. Mehlig, K. Hansen, M. Hedén, A. Lassesson, A. V. Bulgakov and E. E. B. Campbell, *J. Chem. Phys.* ***120****, 4281 (2004)*
Energy distributions in multiple photon absorption experiments

III. M. Hedén, K. Hansen, F. Jonsson, E. Rönnow, A. Gromov, A. Taninaka, H. Shinohara and E. E. B. Campbell, *J. Chem. Phys. accepted*
Thermal radiation from C_N^+ and La@C_N^+

IV. M. Hedén, K. Hansen and E. E. B. Campbell, *Phys. Rev. A accepted*
Molecular fusion of $(C_{60})_N$ clusters in the gas phase after femtosecond laser irradiation

These papers are printed in the Appendix.

The following papers are not included in the thesis

- F. Rohmund, A. V. Bulgakov, M. Hedén, A. Lassesson and E. E. B. Campbell, *Chem. Phys. Lett.* ***323****, 173 (2000)*
Photoionisation and photofragmentation of Li@C_{60}

- A. Lassesson, A. V. Bulgakov, M. Hedén, F. Rohmund and E. E. B. Campbell, *"The Physics and Chemistry of Clusters", Proceedings of Nobel Symposium 117, World Scientific, 2001*
Laser desorption studies of the fragmentation of Li@C_{60}

- F. Rohmund, M. Hedén, A. V. Bulgakov and E. E. B. Campbell, *J. Chem. Phys.* ***115****, 3068 (2001)*
Delayed Ionization of C_{60}: the competition between ionization and fragmentation revisited

- A. V. Bulgakov, O. F. Bobrenok, V. I. Kosyakov, I. Ozerov, W. Marine, M. Hedén, F. Rohmund and E. E. B. Campbell, *Phys. Solid State* ***44****, 617 (2002)*
  Phosphorus clusters: synthesis in the gas-phase and possible cagelike and chain structures

- F. Lépine, B. Climen, F. Pagliarulo, M. A. Lebeault, C. Bordas and M. Hedén, *Eur. Phys. J. D* ***24****, 393 (2003)*
  Dynamical aspects of thermionic emission of C_{60} studied by 3D imaging

- M. Boyle, M. Hedén, C. P. Schulz, E. E. B. Campbell and I. V. Hertel, *Phys. Rev. A* ***70****, 051201 (2004)*
  Two-color pump-probe study and internal-energy dependence of Rydberg-state excitation in C_{60}

- A. V. Bulgakov, M. Hedén, A. Lassesson, K. Mehlig, F. Rohmund and E. E. B. Campbell, *Thermophys. Aeromech.* ***11****, 525 (2004)*
  Decay dynamics of fullerene C_{60} and endofullerene $Li@C_{60}$ molecules excited by laser radiation

- M. Boyle, T. Laarmann, K. Hoffmann, M. Hedén, C. P. Schulz, E. E. B. Campbell and I. V. Hertel, *Submitted to Eur. Phys. J. D*
  Excitation dynamics of Rydberg states in C_{60}: The role of internal energy stored in vibrational modes

The authors contributions to the appended papers.

- Paper I: MH did the experiments and part of the analysis together with AVB. EEBC did the modeling together with KM and wrote the paper.

- Paper II: MH did the experiments together with AVB. KH and KM did the modeling, the calculations and wrote the paper.

- Paper III: MH did the experiments and analysed the data. KH did the modeling. MH and KH wrote the paper.

- Paper IV: MH and KH did the experiments and analysed the data. EEBC wrote the paper.

Preface

Five years is a long time. Especially when the experimental signal is lost, the lasers won't lase, all deadlines clash at the same date, the vacuum pumps break down and the experimental data points look like someone has sneezed on the plot. However, when one gets to discover new things, see new places of the Earth, meet interesting people, learn both practical and theoretical skills and the machines work flawlessly, then times flies. Fortunately the latter dominates. This thesis does not by any means describe all that I have learnt over these years, it merely summarises the most important scientific findings. Many experiences will never be revealed to the general public, like how not to perform many experiments, how to import lasers from Estonia and how many things can go wrong at the same time. Still they are valuable experiences.

This thesis is organised as follows. Chapter 1 is a short introduction in simple words explaining what has been studied and why one can devote five years to do it. This work is all about one type of molecule and Chapter 2 gives a brief background to the special features which are more or less studied in detail. Chapter 3 describes the experimental equipment from a rather technical point of view. Chapters $4 - 8$ describe the experiments upon which this thesis is based, discusses the methods used, the results, interpretations and conclusions. Each of these chapters are supposed to be selfcontained. The experiments are also described in the appended papers (with the exception of the work on Rydberg states). Chapter 9 offers some general conclusions and an outlook into the future of the field.

The thesis is written for people with an interest in the field, a basic knowledge about gas phase clusters or molecules is necessary to appreciate the work. However, the ambition is that the text in the thesis should be fairly easy to follow, while the papers could be a bit more involved.

Here we go.

Contents

Chapter 1

Introduction

Science is a puzzle. The ultimate goal is to find an understanding of our world. As an important biproduct, the standard of living can be improved by the gained knowledge. To obtain this understanding numerous building blocks are needed.

One fairly new type of building block within physics and chemistry is clusters. Clusters consist of atoms, from a few up to several thousands. Clusters are said to bridge the gap between atoms and bulk material, large clusters tend to have properties very similar to the condensed form of the species while smaller clusters are more like atoms/molecules in their behaviour. Cluster research, which has grown in size and interest since its start in the early 1980's, tries to answer questions like when properties of various types of clusters change from bulk like to molecular. The size and wide range of electrical, geometrical and chemical properties that clusters possess also makes them ideal candidates for applications within various fields such as nanotechnology and catalysis.

Carbon is an essential building block of all life on Earth. It provides the framework for the tissue of all living species. More than six and a half million compounds of carbon are known, much more than of any other element. This means that carbon is studied by scientists from almost all fields of natural science, from astronomers to biologists. It even got its very own branch of chemistry. Two forms of carbon can be found in various locations all over the Earth. The one regarded to be the most beautiful is diamond, where the carbon atoms are joined up in regular tetrahedrons. This makes a very hard, but brittle, compound with a high refractive index resulting in a beautiful brilliance. The second form of carbon is graphite. In graphite the atoms are joined in six membered rings creating large, strongly bound sheets. The

sheets are bound together by van der Waals forces. A third form, fullerenes, was found by Kroto and coworkers in 1985 [1]. While doing experiments to try to understand the mechanisms behind the formation of long carbon chains in interstellar space they observed a family of strange carbon clusters of which some, especially the one containing 60 carbon atoms, were extraordinarily stable. Later it was shown that these carbon clusters are in the form of closed cages consisting of pentagons and hexagons. The most stable fullerene, C_{60}, has the same structure as an ordinary football making it very symmetrical, rigid and indeed beautiful. The C_{60} has a radius of 7 Å which actually means that the size difference between the Earth and a football is approximately the same as the difference between a football and a fullerene as illustrated in Fig. 1.1. The C_{60} was named Buckminsterfullerene after the architect

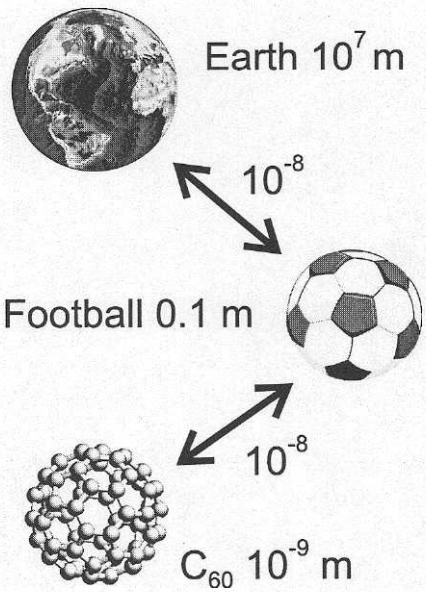

Figure 1.1: The relative difference in size is the same between a fullerene and a football as between a football and the Earth.

R. Buckminster Fuller who had a passion for building geodesic domes, made of pentagons and hexagons. Harry Kroto, Robert Curl and Richard Smalley were awarded the Nobel Prize in chemistry in 1996 for their discovery.

Fullerenes are, strictly speaking, molecules but they do share a lot of prop-

erties with atomic clusters. It is easy to see why these molecules quickly became a popular research object. Not only were they a new form of carbon but they also had an intriguing shape and size which could make them useful in all kinds of applications within microelectronics, nanotechnology, various kinds of chemistry and medicine. As often is the case, most of these weird and wonderful ideas could never be realised but still some applications have sprung from fullerenes and research is continuing. Today the hope for ground breaking new technologies has been largely transferred to the fullerene relatives, carbon nanotubes [2, 3]. Nanotubes can be regarded as rolled up sheets of graphite with a diameter similar to the fullerenes but their length can go up to centimeters. They have electrical and mechanical properties which are very interesting.

The fullerenes are also interesting from a more fundamental point of view. Their simple but ingenious structure makes them relatively easy to handle not only experimentally but also theoretically. Due to their close relationship with clusters, things learned from fullerenes can then be transferred to clusters and more complex molecules. Knowledge which then will be another building block of understanding.

The work presented in this thesis is devoted to the behaviour of fullerenes that have obtained a large amount of energy. It will hopefully contribute to the development of experimental methods and theoretical models for describing atomic clusters and large molecules. Species which, in turn, are one more brick in the framework on which we base our perception of the world.

Chapter 2

Background

The special kind of carbon clusters today called fullerenes were discovered by H. W. Kroto, R. E. Smalley and R. F. Curl and their students J. R. Heath and S. C. O'Brien [1]. By firing a pulsed Nd:YAG laser at a graphite disc in a helium flow they created a large number of carbon clusters of which one containing 60 atoms seemed remarkably stable. The structure that gave such a great stability turned out to be a truncated icosahedron, a polygon with 60 vertices and 32 faces, of which 12 are pentagons and 20 hexagons. This is the very structure of an ordinary football as can be seen in Fig. 2.1. All the molecules with more than 30 atoms seemed to have a cage like structure.

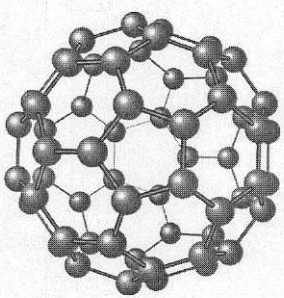

Figure 2.1: The structure of the Buckminsterfullerene, C_{60}.

In 1990 Krätschmer and coworkers succeeded as the first group in the world to produce macroscopic amounts of pure ($\geq 95\%$) C_{60} [4]. The material was

produced by evaporating pure graphitic rods in an atmosphere of helium. A black soot was obtained which was dissolved in benzene, carbon disulphide or some other solvent. The solvent was then dried by a gentle heating. Today C_{60} and C_{70} with a purity $\geq$ 99% are commercially available in powder form, allowing extensive research on fullerenes. Other stable fullerenes can be obtained by purification of fullerene soot which can also be purchased commercially.

2.1 Excitation and relaxation of fullerenes

C_{60} is a highly symmetrical and very rigid molecule which makes it possible to study photophysical processes that can not be studied in many other molecules. Fullerenes have become something of a model system for large molecules/clusters since their structure is fairly simple and they are easy to produce and handle. One interesting feature of C_{60} is that it can absorb photons whose energies add up to a value much greater than the ionisation potential (up to 50 eV) without undergoing immediate ionisation. This creates a highly excited molecule which has several possibilities to get rid of the energy. Ionisation and C_2 evaporation (fragmentation) are the two most prominent decay channels. After a "normal" excitation by ns laser pulses C_{60} will undergo both ionisation and sequential C_2 evaporation. The fullerene can fragment down to C_{32} by C_2 evaporation. These two processes are competing on the timescales of a typical gas phase mass spectrometric experiment. Radiative cooling (photon emission) is a less dramatic decay channel but on the other hand it does not require an activation energy so it is always present (as long as the fullerene is warmer than the surrounding environment). The dynamic behaviour of the decay is dependent on the timescale studied, means of excitation etc. In the case of excitation using laser pulses the pulse duration, photon energy and laser fluence are of course important. The nature of the individual decay mechanisms has to be considered and this is not always perfectly known. Some of the most important issues will be discussed below.

2.1.1 Ionisation

Ionisation is probably the most well known decay mechanism for highly excited gas phase fullerenes but still there are some open questions. The ionisation potential of C_{60} has been measured to be 7.64 eV by single-photon

ionisation using a synchrotron source [5]. The nature of the ionisation process depends on the means of excitation. C_{60}^{12+} has been produced with IR fs laser pulses which is the highest charge state observed today [6]. When exciting gas phase fullerenes with laser light in the near IR – UV wavelength range the energy goes into the electrons and depending on the time scale of the excitation the dynamics of the ionisation changes. This can be illustrated by studying time of flight mass spectra and photoelectron spectra of C_{60} excited with femtosecond laser pulses and varying the pulse length [7]. For pulse durations shorter than ~100 fs ionisation is a coherent multiphoton process. The photoelectron spectra show a clear above threshold ionisation (ATI). When the laser pulses become longer the energy has time to couple to the other electronic degrees of freedom and there is a statistical redistribution of the energy. The ATI structure in the electron spectra is now gone and the energy distribution of the electrons as measured in the photoelectron spectra is less structured. The mass spectra, however, still show prompt ionisation on the μs time scale of the spectrometer. Going to even longer pulses (ps) the energy also couples to the vibrational degrees of freedom. At these pulse durations there is considerable fragmentation of the fullerenes and delayed ionisation can be observed in the mass spectra. Delayed ionisation on the microsecond timescale implies that the energy has been distributed among the vibrational degrees of freedom and at some point enough energy couples back to an electron for ionisation to occur. Delayed ionisation of C_{60} manifests itself as tail on the C_{60}^+ peak in a time of flight mass spectrum as seen in Fig. 2.3. This can be detected up to 100 μs after excitation [8]. Delayed ionisation of neutral C_{60} and C_{70} was discovered in 1991 by Campbell and coworkers [9] (for the first time ever it was observed for metal oxide clusters in 1986 [10]). Today, delayed ionisation has been observed from neutral, negatively and positively charged metal clusters and fullerenes, however only in clusters where the ionisation potential or electron affinity is smaller than the fragmentation energy. The true nature of delayed ionisation has been a subject for discussion for several years, especially the question whether it is purely thermionic or not [11, 12].

The nature of ionisation is obviously connected to electronic excitation and in this thesis two types of excited electronic states in C_{60} get extra attention, the triplet state and the Rydberg states. C_{60} has completely filled electronic shells so in its ground state configuration it does not have a triplet state but if one electron is excited that can have a spin parallel to the un-paired electron in the HOMO giving rise to a triplet state, which is relatively long lived. The lifetime of the triplet state and its possible importance for delayed ionisation is touched upon in Chapter 4.

C_{60} naturally also has high-lying electronic states, Rydberg states. Experimental observation of resolved Rydberg states was reported for the first time by Boyle et al. [13] (Rydberg states in C_{60} have not yet been observed with any other techniques like zero kinetic energy electron (ZEKE) spectroscopy). Gas phase C_{60} was ionised by a 800 nm Ti:Sapphire laser with a pulse duration of 1.5 ps. Energy resolved photoelectron spectra of the electrons emitted in the ionisation process showed distinct peaks due to one photon ionisation of excited Rydberg states. The Rydberg states were excited from the neutral C_{60} and one photon ionised within the same ultrafast laser pulse. The structure could be reproduced using different wavelengths (also 400 nm) and different pulse durations, from 5 ps down to 30 fs where some residual, poorly resolved structure could still be seen. The structure got less detailed with shorter pulses due to the increased bandwidth of the laser. By solving the Schrödinger equation for a jellium like potential for C_{60} and comparing the obtained energy levels to experiments the observed peaks could be determined as coming from ionisation of Rydberg states. The strongest series were $\ell = 5$, $\ell = 3$ and $\ell = 7$. Fig. 2.2 shows photoelectron spectra obtained with three different pulse lengths together with a model fit. In all spectra peaks due to ionisation from Rydberg states can be seen, most clearly for the longest pulse length. The mechanisms behind the excitation of Rydberg states are investigated in Chapter 6.

2.1.2 Fragmentation

The most prominent feature of a mass spectrum of gas phase C_{60} ionised by ns laser pulses is the bimodal fragmentation pattern [14]. If the laser fluence is high enough the spectrum will be dominated by high mass, even numbered carbon fragments C_n^+, $n = 32 - 58$, and lighter carbon clusters C_n^+, $n < 32$, separated by one C mass, as can be seen in Fig. 2.3. The energy required to form the lighter fragments has been measured to be ~85 eV by electron impact ionisation [15]. Mobility studies show that the heavier fragments are still fullerene-like (closed cages) while the lighter fragments, $21 \leq n \leq 29$ are monocycle and multicycle rings and the lightest, $n < 21$ are monocycles or linear chains [16].

The dissociation energy (C_2 evaporation energy) of C_{60} has been the subject of many publications. The published values have ranged from ca 3 up to 15 eV as nicely illustrated in Fig. 3 in Ref. [17]. Up until 1997 most experiments gave a value ≤ 7 eV for the activation energy of the reaction $C_{60}^+ \rightarrow C_{58}^+ + C_2$. The dissociation energy of C_{60} is 0.54 eV higher than for C_{60}^+ [18, 19].

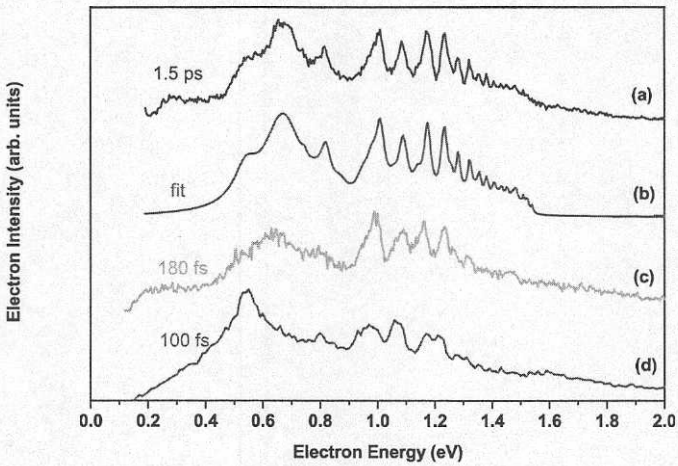

Figure 2.2: Photoelectron spectra from 0 to 2 eV from C_{60} obtained with 800 nm photons. Peaks due to Rydberg states can clearly be seen. **(a)** 1.5 ps, $1.1{\cdot}10^{12}$ W/cm^2, **(b)** best fit to (a), **(c)** 180 fs, $4{\cdot}10^{12}$ W/cm^2, **(d)** 100 fs, $7.5{\cdot}10^{12}$ W/cm^2. Laser bandwidth $\approx$20 meV. Adapted from [13].

Theoretical studies (using Hartree-Fock, tight binding methods, DFT etc.) all gave values $\geq$ 10 eV [20]. After 1997 the experimental values started to grow larger and today they seem to converge around 11 eV. Some of the most recent values are 11.4 eV calculated by DFT (B3LYP/6-31G(d)) [21], 11.2 eV obtained from kinetic energy release distributions [22] and 10.6 eV from analysis of delayed ionisation (the value from Ref. [8] has been reanalysed) [23].

One of the main reasons for the difficulty in determining the dissociation energy in C_{60} is that it can not be measured directly. Fragmentation competes with ionisation and radiative cooling (photon emission) so some modeling and assumptions about the competing processes are necessary. Experiments in 1996 showed that it was crucial to include radiative cooling in the modeling, an effect which has very often been neglected [24]. Another source of problems was the pre-exponential factor for ionisation and for fragmentation (very often the decay rate is given in an Arrhenius form, $k = Ae^{-E_a/(k_B T)}$, where E_a is the activation energy, k_B Boltzmanns constant, T the temperature and A the pre-exponential factor). It is convenient to set the Gspann

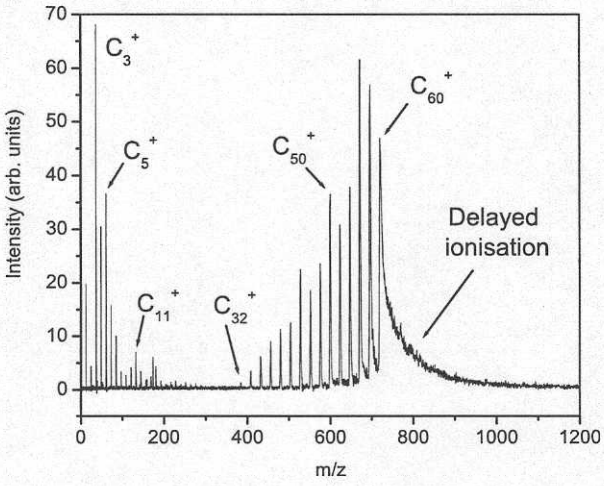

Figure 2.3: A typical time of flight mass spectrum of C_{60}. C_{60} powder was evaporated at 460 °C and the created vapour was ionised by a strongly focused ns N_2 laser (337 nm). The heavy even numbered cage-like fragments C_n^+, $n = 32-58$, are clearly seen together with the smaller fragments which are both odd and even numbered. There is also a distinct tail on the C_{60}^+ peak due to delayed ionisation.

parameter[1] to a constant and this has been done frequently but often a too low value has been used and in some cases the approximation of a constant Gspann parameter is not a good one.

2.1.3 Radiative cooling

As mentioned above, radiative cooling from excited gas phase fullerenes has often been ignored in analyses of experimental data not to add further complexity to the problem or has been implemented incorrectly. However, as the work in Ref. [24] showed, in many cases the cooling by radiation has to

[1]Decay rates are often written in an Arrhenius form, $k = Ae^{-E_a/(k_B T)} \Leftrightarrow ln(A/k) = E_a/(k_B T) = G$, where G is called the Gspann parameter [25].

be considered. Photon emission from fullerenes suffers from the same problem as C_2 emission; it is very hard to measure radiative cooling directly, usually there are competing decay channels that have to be modeled correctly in order to get a good estimate of the emitted radiation. There are a few measurements of the actual emission spectrum from excited fullerenes, e.g. [26, 27]. Photon emission from fullerenes will be addressed further in Chapter 7.

2.2 Endohedral fullerenes

Together with the discovery of the fullerenes other species were observed with masses corresponding to fullerenes plus one extra atom [1, 28]. It was shown that one (or more) atoms could be trapped inside the fullerene cage. The centre of fullerenes provides an exceptionally strong binding site for a wide range of atoms, while other atoms (e.g. N) only interact weakly with the cage. The extra atom naturally alters the properties of the fullerene. If there is a charge transfer from the endohedral atom to the cage the electronic properties are changed which could be interesting. Heath et al. produced a small amount of fullerenes with a La atom inside the cage in 1985 by the same means as the first fullerenes were produced, the only difference being that the graphite had been impregnated with lanthanum [28]. Mass spectra showed the presence of La@C_n, where n is an even number from 44 to over 76 (the @ indicates that the atom is inside the fullerene). The La@C_n complexes were more stable than the bare C_n clusters (with the exception of C_{60}) indicating that the endohedral atom helps to stabilise the complex.

Endohedral fullerenes are today normally produced either by laser desorption or arc burning of graphite containing some additional atom, by collisions between a fullerene beam and an atomic/molecular beam or by irradiating a thin film of fullerenes with an ion beam, see Refs. [14, 29] and references therein. The main difficulty with endohedral fullerene production is the extraction and purification of the produced species. The most studied endohedral fullerenes are rare earth metals confined in C_{82}, such as La@C_{82}. They are normally produced by arc discharge and are fairly easy to dissolve and purify by high pressure liquid chromatography (HPLC). However, only certain species can be extracted from the soot. Endohedral forms of C_{60} are problematic to extract in a pure form but it is by no means impossible. A method based on the irradiation of films of C_{60} or C_{70} by ions was developed in 1996 by Tellgmann et al. [30, 31]. Fullerenes are deposited on to a sub-

strate which is then exposed to a low energy ion beam, usually Li^+. The ions penetrate the carbon cage and are trapped inside the cage. The fact that the fullerenes are deposited on a surface helps the formation of endohedral complexes since the vibrational energy transferred to the cage in the capture of the ion can be dissipated to the bulk, inhibiting fragmentation of the cage. The films can be further purified by means of HPLC [32]. After purification more than 90% of the sample is $Li@C_{60}$. The availability of larger amounts of $Li@C_{60/70}$ has given the possibility to make further characterisation and studies of these species [33, 34]. It is also possible to use the described method to produce endohedral fullerenes containing other alkalis.

In this thesis it is examined how the endohedral atom of $La@C_{82}$ influence the radiation behaviour of the excited molecule compared to empty fullerenes (Chapter 7).

Chapter 3

Experimental equipment

3.1 Reflectron time of flight mass spectrometry

All of the experiments presented in this thesis were performed in a reflectron time of flight mass spectrometer (ReToF). Time of flight mass spectrometry is a quite simple but still efficient way to mass resolve ions in the gas phase. Depending on the configuration it is possible to achieve mass resolution better than one atomic unit for a large range of masses. It also has the advantage that it can collect the entire mass spectrum in one single shot. The species to be investigated are ionised in the middle of a static (or pulsed) electric field. The electric field will accelerate the ions into a field free region at the end of which the ions are detected by a detector, usually a microchannel plate (MCP) or microsphere plate (MSP) detector. The ion counts are recorded with respect to their arrival time at the detector by an oscilloscope or a single ion counter card (in this work). A schematic view of the ReToF mass spectrometer in Göteborg is shown in Fig. 3.1. The spectrometer consists of two differentially pumped vacuum chambers, the interaction chamber and the flight chamber. In the acceleration stage the ions will achieve an energy $E = qU$ where q is the charge of the ion and U the accelerating potential. This energy is transferred into kinetic energy $qU = \frac{1}{2}mv^2$. The velocity of the ions, and their flight time in the spectrometer, is thus only dependent on their charge q and mass m. So by recording the time of flight for an ion it is possible to assign a mass to charge ratio to it. However, variations in the initial space and velocity distributions of ions with the same value of q/m will result in different arrival times at the detector, broadening the mass peaks. The spatial resolution can be improved by giving the ions a velocity

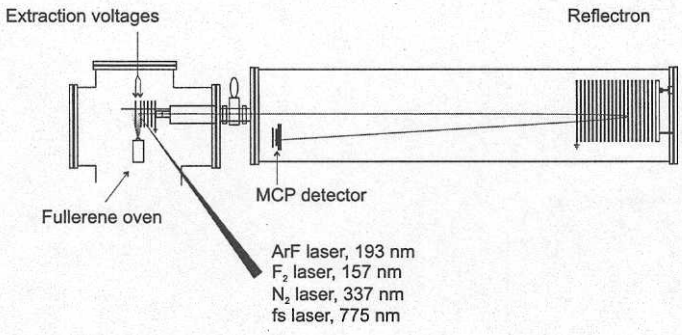

Figure 3.1: Schematic view of a reflectron time of flight mass spectrometer.

dependent on their starting position, so that ions created farther from the detector will get a higher velocity than the ones created at a shorter distance. This is usually done by tuning the shape of the accelerating potential (Wiley-McLaren ion optics) [35]. The broadening of the mass peaks due to the initial velocity distribution of the ions can be reduced by using a reflectron [36, 37]. The idea is to use two electric fields to reflect the ions after they have passed a field free region. One electric field slows down the ions, another field reflects them and they are then accelerated by the first field again. They pass the field free region once more and are then detected. The ions with a high initial velocity will spend more time in the reflectron than ions with a low initial velocity. In this way, focusing with respect to the initial velocity distribution can be obtained by setting the voltages in the reflectron so that ions with the same ratio m/q will have the same time of flight.

The reflectron can be tuned to focus ions undergoing metastable fragmentation (fragmentation in the first field free region) onto the same mass peak as the ions not undergoing this fragmentation. It can also be set to separate the metastable peaks from the "parent" peaks, even though this usually means loss of overall resolution.

The principle of operation for a time of flight mass spectrometer means that it can not only determine the mass to charge ratio of ions in the gas phase but it can also be used to study their behaviour on a μs timescale, i.e. things like metastable fragmentation, delayed ionisation, lifetimes of excited molecular states etc. Fig. 3.2 gives an example of the time scales involved in a typical experiment on C_{60} in a ReToF.

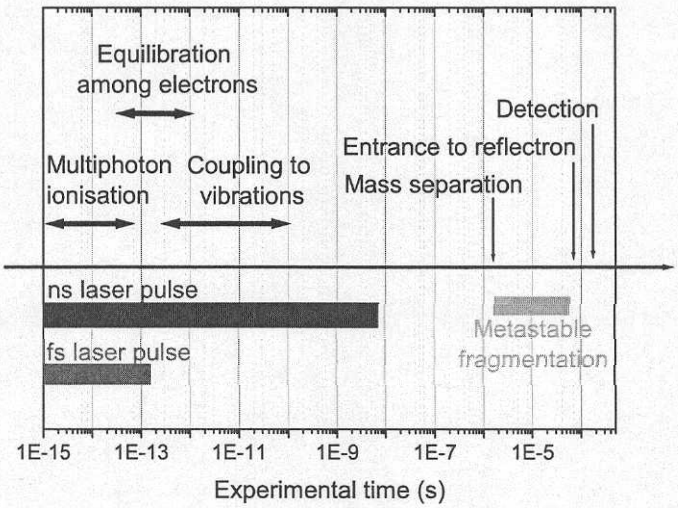

Figure 3.2: Typical experimental time scales for photoionisation experiments with fullerenes in a reflectron time of flight mass spectrometer where the excitation comes from a fs or a ns laser. The figure should merely give a feeling for approximate time scales. Note the logarithmic time axis.

The ion and electron time of flight spectrometer at MBI

Time of flight spectrometry can also be performed on electrons. A photoelectron time of flight spectrometer can be used to determine the energy of the electrons emitted from atoms or molecules in the ionisation process induced by a laser pulse. The spectrometer used for the experiments on Rydberg states in C_{60} described in Chapter 6, located at the Max-Born-Institute for Nonlinear Optics and Short Pulse Spectroscopy in Berlin, is a combination of a reflectron time of flight mass spectrometer and an electron spectrometer. The ReToF is almost identical to the one described above and the electron spectrometer is situated on the opposite side of the extraction region from the mass spectrometer. The electron spectrometer does not use any applied extraction fields, the electrons are only driven towards the detector by the electric field of the laser. The principle is very similar to that of the mass spectrometer; electrons with a high energy will reach the detector first, followed by less energetic electrons allowing an energy spectrum to be recorded. It is not possible to measure ions and electrons simultaneously, but the switching from one mode to the other is very quick so both measurements

can be performed under identical conditions.

3.2 The Cold Source

C_{60} has a rather large heat capacity which makes it difficult to reach low vibrational temperatures in the gas phase. One way to achieve this, however, is to use a gas aggregation source. In a gas aggregation source fullerenes (or molecules, atoms etc.) are vapourised in a slowly streaming carrier gas (typically He or Ar). The gas is cooled by collisions with the chamber walls which are cooled with liquid nitrogen. The fullerene vapour is quenched by the gas and transported through a nozzle with a temperature of 80 – 100 K. This will create fullerenes with a vibrational temperature of 80 – 100 K or lower. The beam will have a speed of about 700 m/s [38]. If the density of the fullerenes (atoms, molecules) is high enough they will also tend to aggregate into clusters [39]. The gas aggregation source used in the experiments described here (the Cold Source) has a conical nozzle with a diameter of 2 mm. The temperature of the nozzle is monitored by a thermocouple. The beam goes through a 3 mm diameter skimmer and a differential pumping stage before it enters the interaction region of the time of flight mass spectrometer where it can interact with laser light and be studied. The Cold Source has previously been used to study clusters of fullerenes [40, 41] (and on one occasion clusters of phosphor [42]). In this work it has been a source of both clusters of fullerenes and vibrationally cold monomers of C_{60}. A schematic picture of the Cold Source is shown in Fig. 3.3.

3.3 The lasers

Different lasers have been employed in this work. The one used in most of the experiments is a commercial (Laser Science Inc. VSL337ND-S) pulsed N_2-laser. The output wavelength is 337 nm (3.68 eV) and the pulse duration is < 4 ns. The repetition rate can be varied between 0 and 60 Hz. The average power is > 7.2 mW at 30 Hz.

Together with the N_2-laser a commercial (Neweks Ltd. PSX-100) excimer laser has been used. The laser medium has been an ArF gas mix giving an output wavelength of 193 nm (6.42 eV) or an F_2 gas mixture which gives 157

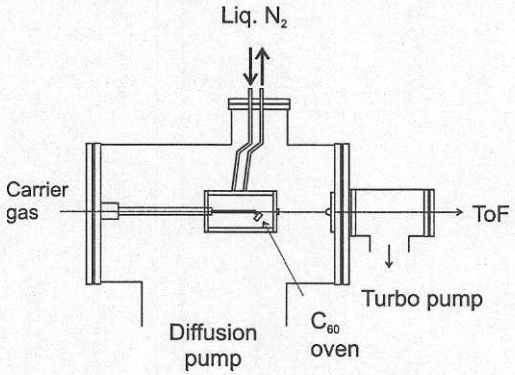

Figure 3.3: The Cold Source. A gas aggregation source for production of a beam of clusters or vibrationally cold fullerenes.

nm (7.90 eV). With 7.9 eV photons it is possible to single photon ionise C_{60}. The pulse duration is typically 5 ns and the average power is specified to 350 mW when the laser is used with ArF. The repetition rate goes up to 100 Hz.

The experiments on molecular fusion of $(C_{60})_N$ clusters involved a commercial Ti:Sapphire femtosecond laser system, Clark-MXR CPA-2001. The pulse length is 150 fs as it comes out of the laser, the pulse length is stretched on its way to the interaction chamber (which in Göteborg is unusually long). The typical output power for the fundamental (775 nm) is 900 mW at 1 kHz repetition rate. The repetition rate can be varied from 10 Hz to 1 kHz. The laser system is also equipped with a NOPA (Non-linear Optical Parametric Amplifier) which can generate tunable light in the range $450-700$ nm, $870-1600$ nm. The pulse durations are < 30 fs at $450-700$ nm and < 50 fs at $870-1600$ nm. Output power from the NOPA is between 2.5 and 12 mW at 1 kHz depending on wavelength.

The work on Rydberg states in C_{60} was performed at the "kHz Clark" system at the Max-Born-Institute. The laser system is based on a Ti:Sapphire fs-laser/amplifier system (Clark MXR) similar to the one described above. The system can deliver sub 100 fs laser pulses tunable between $780-830$ nm with a single pulse energy of about 600 μJ. It is also possible to achieve shorter wavelengths by second-, third-, and fourth harmonic generation.

Chapter 4

Lifetime of the C_{60} triplet state

As mentioned in Chapter 2, there has been a discussion in the literature whether delayed ionisation from fullerenes is a truly thermionic process or not. Thermionic emission is a completely statistical process where the excitation energy is distributed among all degrees of freedom. Over the years there have been indications both for and against a completely statistical description, see e.g. Refs. [11, 43, 44].

In Ref. [45] a closer look was taken at delayed ionisation. The ionisation of laser excited C_{60} was simulated using the most common decay rates for ionisation, fragmentation and radiative cooling at the time. The simulations were compared to experimental data where C_{60} had been excited by a 337 nm laser and then examined in a reflectron time of flight mass spectrometer. The laser was focused to just barely cause the appearance of small, non-fullerene like fragments in the mass spectrum. Hansen and Echt have shown that delayed ionisation follows a power law in time, $I = I_0 t^{-p}$, $p = 0.64 \pm 0.1$, at least up to 10 μs after excitation [44]. It turned out to be very difficult to reproduce the shape of the delayed ionisation tail from the calculations, while the experiments confirmed such a power law. After 10 μs however the measured electron emission rate drops off and deviates from the power law. Ref. [45] raised some questions about the accuracy of the assumptions about pre-exponential factors, internal energy and dynamics but also noted a possible solution. By introducing ionisation from the triplet state the experimental data could be fitted reasonably well. By also assuming that the triplet state undergoes an exponential decay back to the singlet ground state with a lifetime of some tens of μs the observed drop off in the electron emission rate could be roughly described. The lifetime of the triplet state of

C_{60} from a laser vaporisation source has been determined to be 42 μs [46]. Using this value in the calculations gave quite a nice fit to the experimental data. The transition from the triplet ground state to the singlet ground state is actually forbidden due to symmetry reasons but the symmetry is broken by vibrations so the transition becomes weakly allowed. Thus the amount of vibrational energy might be of great importance for the lifetime of the triplet state. The excitation energy of the C_{60} in Ref. [46] was assumed to be much lower than in the work described in Ref. [45]. Haufler et al. assumed that the C_{60} was excited by one 4 eV photon and that any vibrational excitation was quenched by the supersonic expansion in the vaporization source. Other work has been done on the triplet lifetime at a range of higher excitation energies (~5-9 eV) [47]. At these higher energies much shorter lifetimes were measured. The experiments were done on C_{60} vapour in an Ar buffer where the buffer gas could be heated to a desired temperature between 979 and 1040 K. The vapour was excited by a ~4 mJ pulse of 532 nm photons from a Nd:YAG laser. The triplet state was then probed by looking at the absorption of a continuous 758 nm diode laser. The analysis of the experiments suggested that the decay rate of the triplet state $k_{T\rightarrow S}$ was strongly dependent on the vibrational excitation energy and was given by

$$k_{T\rightarrow S}(E_{vib}) = B \exp[\alpha E_{vib}], \tag{4.1}$$

where $B = 3290$ s^{-1} and $\alpha = 0.8$ eV^{-1}. If one extrapolates these results to lower energies the 42 μs measured by Haufler et al. and other measurements of the triplet state lifetime done in room temperature solutions [48] and low temperature glass [49, 50] fall rather nicely on to this line as seen in Fig. 4.1. Extrapolating towards the higher energies relevant for the experiments on delayed ionisation would give a decay rate $k_{T\rightarrow S}$ around 10^{10} s^{-1}, which is much too high to explain the experiments. However, in the experiments of Etheridge et al. there are a lot of collisions between the C_{60} and the buffer gas within the lifetime of the triplet state leading to collisional relaxation of the excess vibrational energy. Thus the situation could be quite different for collision free molecular beam experiments. It would therefore be of interest to measure this lifetime under the same experimental conditions used during the measurements of delayed ionisation in Ref. [45].

4.1 Experimental

To get an estimation of the triplet state lifetime of excited C_{60} in the gas phase a pump-probe technique was used. The experiments were performed

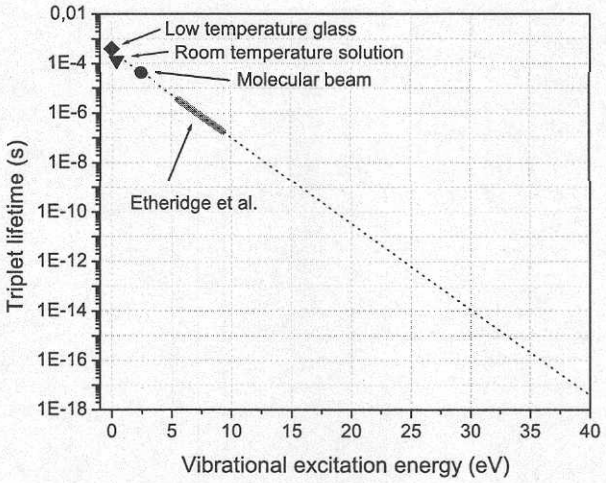

Figure 4.1: Lifetime of the triplet state in C_{60} as a function of vibrational excitation energy. The thick solid line is the work done by Etheridge et al. [47], the diamond is from experiments in low temperature glass [49, 50], the triangle from room temperature solution [48] and the circle is from measurements on a molecular beam [46]. The dotted line is an extrapolation of the Etheridge results.

in the same ReToF chamber (described in Chapter 3) as the work on delayed ionisation. C_{60} (99.5% purity) was heated to typically $460 - 500$ °C in an effusive oven placed under the acceleration grids in the interaction chamber. The N_2 laser was used to pump the gas phase C_{60} into the triplet state. The laser has a photon energy of 3.7 eV which means that if one such photon is absorbed by a C_{60} an intermediate singlet state will be occupied. This state will rapidly decay down to the triplet manifold on the order of nanoseconds [51–53]. The ArF laser, working as probe, was fired with a time delay with respect to the pump laser. That laser has a photon energy of 6.4 eV, so one photon is enough to ionise the C_{60} if it is still in the triplet ground state, which lies 1.7 eV above the singlet ground state [54]. However, if the triplet state has decayed back to the ground state 6.4 eV is not enough to ionise the system and it will not be detected in the spectrometer as illustrated in Fig. 4.2. By scanning the delay between the two laser pulses and observing the size of the mass peak produced by the probe pulse one can monitor the

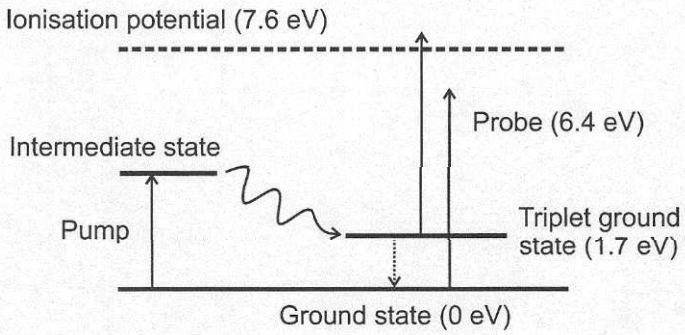

Figure 4.2: The pump laser excites an intermediate singlet state which decays to the triplet manifold on a ns timescale. If the C_{60} molecule is in the triplet state one 6.4 eV photon from the probe laser is enough to ionise it. However, if the molecule has decayed from the triplet state to the singlet ground state during the delay time between the pump and the probe laser pulse, 6.4 eV is not enough for ionisation and no signal will be seen from one photon absorption from the probe laser.

population of the triplet state as a function of time after excitation. It is of importance that the lasers are stable in time with respect to output power and therefore the output power of the probe laser, that showed some instability, was monitored by doing every fourth measurement with only the ArF laser and controlling the signal produced. The probe laser alone does produce some signal since the intensity of that laser was not turned down so much that only one photon absorption was achieved. This naturally has to be considered in the analysis of the data. The lasers were aligned collinearly using a dichroic mirror and they were focused so that the path of the probe laser was always contained within the beam of the pump laser in the extraction region of the mass spectrometer. Various different configurations were used to minimise any geometrical effects. Data sets were collected using different intensities of the pump laser. The intensity was varied by using filters inserted in the beam path. The third harmonic of a Nd:YAG laser (355 nm) was also used as pump laser for comparison. In this case it was possible to work with a pump laser beam covering almost the entire extraction region in the spectrometer ($\sim \phi 12$ mm).

4.2 Results and Discussion

A typical mass spectrum from a pump-probe measurement obtained as described above is shown in Fig. 4.3 (a). The delay between the pump and the probe pulse is 1.3 μs and the fluence of the N_2 laser acting as pump is $\sim$45 mJ/cm^2. Such a fluence is enough for the pump laser to cause ionisation and fragmentation of the fullerenes on its own. 1.3 μs after the C_{60}^+ peak there is a peak (on top of the delayed ionisation) produced from the ArF laser which serves as probe. The size of the peak is proportional to the population of the triplet state. The area of the probe peak was obtained by subtracting a fit of the delayed tail and then integrating over the peak. This was done for all delay times. The values were adjusted for the peak produced by the probe pulse alone and for variations in the probe laser intensity and detection efficiency. The integrated peak intensities are plotted in a lin-log diagram in Fig. 4.3 (b). The dashed line is a single exponential fit to the data. The fitted lifetime for such an exponential decay is 1.3$\pm$0.1 μs. Fig. 4.3 (c) shows a similar mass spectrum as Fig. 4.3 (a) (delay 1.3 μs) but obtained with a much lower laser fluence ($\sim$14 mJ/cm^2). No ions from the pump laser alone are seen, only the peak due to the probe laser. The corresponding corrected probe peak areas are displayed in Fig. 4.3 (d). A single exponential fit shown by the dashed line gives a lifetime of 1.4$\pm$0.1 μs. The given errors are the errors of the least square fit, not the true error in lifetime. Taking all possible errors into account the triplet lifetime in the two cases can be considered to be on the order of 1 μs. The experiments with the Nd:YAG laser as pump gave the same lifetime. Studying the pump-probe signal as a function of probe laser fluence showed that the signal intensity increases linearly with increasing laser fluence indicating that ionisation indeed is a one photon process from the triplet state.

Considering the strong dependence on the internal excitation energy seen by Etheridge and coworkers [47] it would be of interest to estimate the vibrational energy in Fig. 4.3 (a) and (c) respectively. In Paper I the internal energy in the high fluence case was estimated by studying the fragmentation pattern and fitting the delayed ionisation tail (a fit which is sensitive to energy). The energy distribution was assumed to be a Poisson distribution and a mean value of $\sim$30 eV and a FWHM of 25 eV was obtained. For the lower fluence no ionisation or fragmentation from the pump pulse alone was observed so only an upper limit of 15 eV could be assigned. For such internal vibrational energies the lifetimes of the triplet state of $\sim$1 μs does not fall onto the exponential curve of Etheridge et al. shown in Fig. 4.1. Possible reasons for this are thoroughly discussed in Paper I.

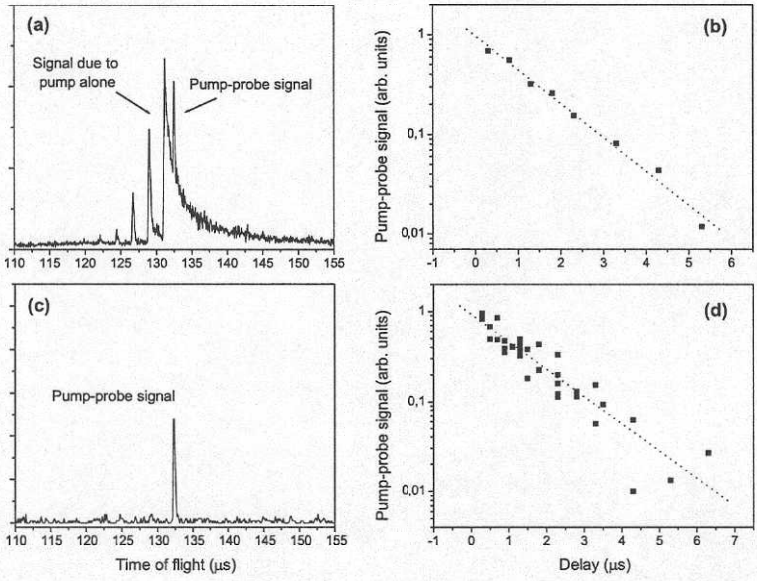

Figure 4.3: Pump-probe measurements of the triplet state obtained at a laser fluence of ~45 mJ/cm^2 (a) & (b), and ~14 mJ/cm^2 (c) & (d). **(a)** Typical ToF mass spectrum at a 1.3 μs delay between the pump and probe laser. **(b)** The signal intensity from the triplet state as a function of delay time. Same conditions as in (a). The dashed line is a single exponential fit giving a lifetime of ~1.3±0.1 μs. **(c)** ToF mass spectrum at a 1.3 μs delay. **(d)** The signal intensity from the triplet state as a function of delay time for the same conditions as (c). The dashed line is a single exponential fit giving a lifetime of ~1.4±0.1 μs.

Measurements of the C_{60} triplet lifetime under very similar experimental conditions were performed by Deng et al. [55] slightly later than the ones described above. They also observed a triplet state lifetime of ~1 μs after excitation by a Nd:YAG (355 nm) laser and probing with an ArF laser (193 nm) but their interpretation of the vibrational energy was different. If the triplet state lifetime depends exponentially on the vibrational excitation as suggested by Etheridge et al. then C_{60} with a vibrational energy of 30 eV would have a triplet lifetime of ca. 11 fs, a time that would not be detectable in the present experiments. Deng et al. assumed that the observed signal

originated from the part of the fullerenes which only absorbed one pump photon, thus their vibrational energy would be the thermal energy obtained in the oven plus the energy of one photon. For higher fluences similar to the high fluence regime in Paper I they also observed a superposition of two different lifetimes in their plots. For short delays between pump and probe a lifetime of 0.041 μs was visible which was attributed to absorption of two pump photons. If such energies are used the measured lifetimes falls close to the exponential curve. Further studies by Echt and coworkers supported this model [56]. By varying the oven temperatures and using lasers with different wavelengths (266, 355 and 532 nm) they varied the vibrational energy of the fullerenes and the measured triplet lifetimes showed an exponential dependence on the vibrational energy as expected. A fit of their data as a function of vibrational energy gave the relationship

$$\tau = \beta \exp(-\alpha E_{vib}), \tag{4.2}$$

where τ is the triplet lifetime, E_{vib} the vibrational energy, $\beta = 78.3 \pm 9.7$ μs and $\alpha = 0.76 \pm 0.02$ eV^{-1}. The fit is shown in Fig. 4.4 together with the fit from Etheridge et al. [47]. In Fig. 4.4 is also included three triplet lifetimes from measurements in low temperature glass [49, 50], room temperature solution [48] and the molecular beam result of Haufler et al. [46]. The vibrational energies in these experiments are read off from Fig. 3 in Ref. [47].

The vibrational energies from Paper I can be reanalysed with the formula given in Ref. [56]:

$$E_{vib} = E(T_{C60}) + nh\nu - E_T, \tag{4.3}$$

where $E(T_{C60})$ is the vibrational energy from the oven, n the number of absorbed photons, $h\nu$ the photon energy and E_T the energy of the triplet state. In Ref. [56] the triplet state energy was set to $E_T = 1.57$ eV[1]. $E(T_{C60})$ was calculated according to

$$E(T_{C60}) = -2.550 + 0.00737T + 2.6523 \cdot 10^{-6}T^2, \tag{4.4}$$

where $E(T_{C60})$ is given in eV and T in K. Eq. 4.4 is a quadratic fit from 600 – 1200 K of a caloric curve calculated from published vibrational frequencies. It should be noted that the fullerenes giving rise to the "pump alone" signal have a considerably higher internal energy than the fullerenes responsible for the pump-probe signal since they originate from different parts of the

[1] $E_T = 1.57$ eV [57] is the value used by Echt et al. but quite often a value of $E_T = 1.7$ eV is used [54]. In the following discussion 1.57 eV will be used for comparison.

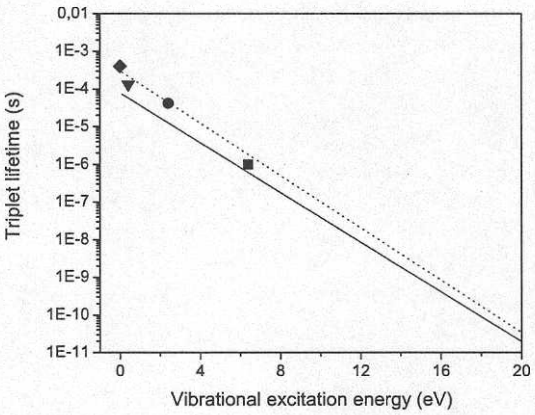

Figure 4.4: Lifetime of the triplet state in C_{60} as a function of internal vibrational energy. The solid line is a fit of the data of Echt and co-workers [55, 56] and the dashed line is the fit of Etheridge et al. [47]. The diamond, triangle and circle are from measurements in low temperature glass [49, 50], room temperature solution [48] and a molecular beam [46]. The square is the data from Paper I, where the vibrational energy content has been reanalysed.

internal energy distribution of the fullerene ensemble. Assuming one 337 nm photon absorbed, a triplet lifetime of 1 μs and an oven temperature of 460 °C gives the square in Fig. 4.4. The triplet lifetime for C_{60} which has absorbed two 337 nm photons would according to Eq. 4.2 have a lifetime of $\sim$0.08 μs. Such a short lifetime would not have been detected since short enough delays between pump and probe pulse were unfortunately not used.

4.3 Concluding remarks

The lifetime of the triplet state in C_{60} is too short to explain the drop off of the delayed ionisation tail observed in several experiments. More recent experiments done in Aarhus with an experimental setup where the fullerene beam and the laser beam are parallel (the laser shoots into the oven) does not show any dramatic decrease in the delayed electron emission rate after 10 μs [8]. It would thus seem that the observed drop off is due to loss of the ions

in the spectrometer. The delayed ionisation tail deviates from a power law due to radiative cooling but that can be reasonably well modeled. Since the publication of Ref. [45] more precise knowledge about dissociation energies, pre-exponential factors, internal energies and such has been gained and now the delayed tail can be satisfactorily modeled. Most of the work today (with some possible exception [58]) points towards microsecond delayed ionisation of fullerenes being truly thermionic.

The difference in the interpretation of the internal energy dependence of triplet state lifetime in Paper I and Ref. [55] shows the importance and difficulties of estimating the internal energy of molecules after laser excitation. Exciting molecules or clusters in the gas phase by a more or less focused laser beam has frequently been assumed to give the ensemble of molecules a Poisson like internal energy distribution. However, it is not at all clear that this is reasonable for a realistic laser beam profile. These issues are pursued in Chapter 5 and Paper II.

Chapter 5

Internal energy distributions of laser excited fullerenes

When different kinds of exponential decay of molecules are studied, an estimation of the energy of the decaying species is always necessary since the decay depends strongly on the energy. In molecular beam experiments laser pulses are the favourite means of excitation for many researchers. In many cases absorption of several photons is needed to reach the desired degree of excitation. However, at higher laser fluences it is very hard to determine the exact number of photons absorbed by the molecules. Naturally not all of the molecules will absorb the same number of photons, there will be an energy distribution in the ensemble of excited molecules. A broad internal energy distribution can give a very different decay behaviour for excited molecules and clusters, considering the ensemble as a whole, as compared to a narrow distribution. This was for example shown in Ref. [59] where an isolated ensemble of clusters with a broad internal energy distribution exhibited a $1/t$ decay rather than an exponential decay which would have been the case for a narrow internal energy distribution.

Very often laser excitation has been assumed to give a Poisson-like internal energy distribution for a molecular ensemble, e.g. Refs. [45, 60]. As seen in Section 4.2 a Poisson distribution is actually not a good representation of the internal energy distribution. It would therefore be of interest to investigate the distribution of the number of absorbed photons in experiments where molecular beams are excited by laser pulses to get a better estimation of the internal energy of the molecules. This was done by calculating the probability of a molecule in a beam absorbing n photons from a Gaussian laser beam

considering the focusing of the laser and the inhomogeneity of the molecular beam.

5.1 Theoretical description of multiple photon absorption

The probability of absorbing n photons with the energy E_{ph} at a laser fluence F and with a constant photoabsorption cross section σ can be described by a Poisson distribution

$$P_n = e^{-\lambda}\frac{\lambda^n}{n!}, \tag{5.1}$$

where $\lambda = \sigma F/E_{ph}$. In most cases the laser beam intensity will not be constant but will vary in space which also will affect the photon absorption. In the simplest case considered here the laser beam will have a Gaussian profile and the beam will be assumed parallel. The density of the molecular beam will be assumed to be constant. The parameter λ will then behave like

$$\lambda(r) = \lambda_0 e^{-2r^2/w_0^2}, \tag{5.2}$$

where r is the radial distance from the center of the laser beam, w_0 the laser beam width and $\lambda_0 = \sigma F_0/E_{ph}$, F_0 being the maximum fluence. Integrating P_n over r gives the total number of molecules that will absorb n photons:

$$I_n \propto \int_0^\infty rdrP_n = \int_0^\infty rdre^{-\lambda(r)}\frac{\lambda(r)^n}{n!} = \int_0^\infty rdre^{-\lambda_0 e^{-2r^2/w_0^2}}\frac{(\lambda_0 e^{-2r^2/w_0^2})^n}{n!}. \tag{5.3}$$

Since the molecular beam density was assumed to be constant it has been omitted in the equation. For high fluences, i.e. $\lambda_0 \to \infty$, I_n approaches n^{-1}. For more moderate fluences I_n is still proportional to n^{-1} up to a cutoff at λ_0 where it drops off roughly following a Poisson distribution (Eq. 5.1) with $\lambda = \lambda_0$ as illustrated in Fig. 5.1.

The laser beam does not only vary in intensity in the radial direction but also along the direction of propagation, especially if it is strongly focused. Calling the direction of propagation z, the width of the beam will be

$$w(z) = w_0\sqrt{1 + \frac{z^2}{z_0^2}}, \tag{5.4}$$

where w_0 is the width at the focal point and z_0 is the Rayleigh range (which is a measure of the inverse divergence). The fluence accordingly goes as

$$F(z) = F_0\frac{w_0^2}{w(z)^2}, \tag{5.5}$$

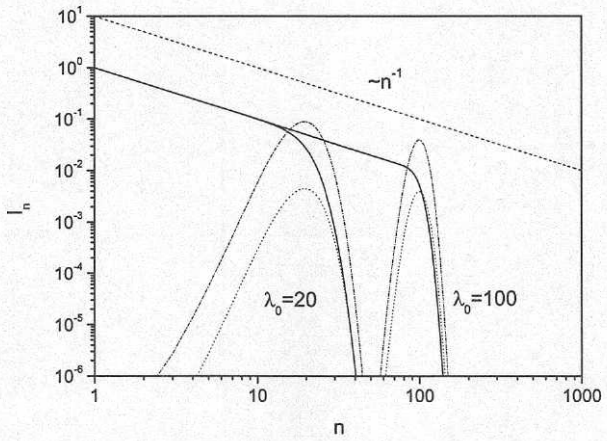

Figure 5.1: Probability of absorbing n photons from a Gaussian laser beam according to Eq. 5.3 (solid lines). The dash-dotted line gives the distribution according to a Poisson distribution with a constant λ (Eq. 5.1). The cutoff at higher n is best described by the Poisson distribution P_n/λ_0 (dotted lines). The dashed line illustrates a gradient $\sim n^{-1}$.

where F_0 is the fluence at the focal point $z = 0$. To get the absorbed energy the distribution of photons has to be weighted with the distribution of molecules. From an effusive source one can expect the molecular beam to roughly have a Gaussian profile in the radial direction. If the molecular beam crosses the laser beam at right angles the density of molecules can be described as

$$I_{mol} \propto e^{-(z-z_v)^2/2r_0^2}, \tag{5.6}$$

where z_v is the distance from the center of the molecular beam to the laser focus and r_0 is the radius of the molecular beam as shown in Fig. 5.2. Assuming that the laser beam is small (narrow) compared to the molecular beam the expression in Eq. 5.3 will be modified by the non-homogeneity of the laser and molecular beam to give

$$I_n \propto \int_{-\infty}^{\infty} dz w(z) e^{-(z-z_v)^2/2r_0^2} \int_0^{\infty} r dr \frac{\lambda(r,z)^n}{n!} e^{-\lambda(r,z)}, \tag{5.7}$$

with $\lambda(r,z) = \lambda_0 w_0^2/w(z)^2 \exp[-2r^2/w(z)^2]$ and $\lambda_0 = \sigma F_0/E_{ph}$. To be able to

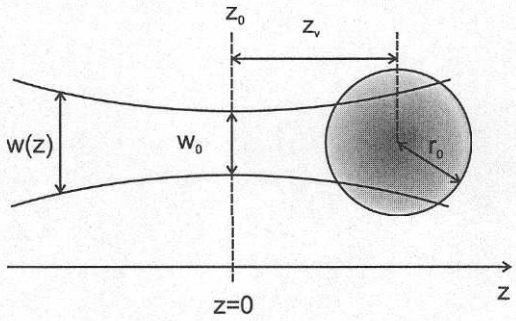

Figure 5.2: Geometry of the laser beam and the molecular beam. The laser propagates in the z direction and is crossed at right angles by the molecular beam (shaded circle). The laser beam waist is placed at $z = 0$.

perform a qualitative discussion some variable changes prove helpful. Transforming $u = \lambda(r, z)$ gives

$$I_n \propto \int_{-\infty}^{\infty} dz w(z^2) e^{-(z-z_v)^2/2r_0^2} \int_0^{\lambda_0 w_0^2/w(z)^2} du \frac{e^{-u} u^{n-1}}{n!}. \tag{5.8}$$

A further variable change of $x \equiv z/z_0$ renders

$$I_n \propto z_0 \int_{-\infty}^{\infty} dx (1+x^2) e^{-(x-x_v)^2 z_0^2/2r_0^2} \int_0^{\lambda_0/(1+x_v^2)} du \frac{e^{-u} u^{n-1}}{n!}. \tag{5.9}$$

Two limiting cases will be investigated, where z_0/r_0 is either small or large compared to unity. The first case, with $(z_0/r_0)^2 \gg 1$, means an almost parallel laser beam (small divergence) which in turn means that x is close to x_v. Putting $x = x_v$ gives

$$I_n \propto \sqrt{2\pi} r_0 (1+x_v^2) \int_0^{\lambda_0/(1+x_v^2)} du \frac{e^{-u} u^{n-1}}{n!}, \quad (z_0/r_0)^2 \gg 1. \tag{5.10}$$

When n is (sufficiently) small one can write

$$I_n \propto \sqrt{2\pi} r_0 (1+x_v^2) \frac{1}{n}, \quad (z_0/r_0)^2 \gg 1, \quad n \ll \frac{\lambda_0}{1+x_v^2}. \tag{5.11}$$

Not surprisingly, the case with a laser beam with a small divergence is very similar to the parallel beam case. One of the differences is that the cutoff at high n is determined by the distance between the laser focus and the

molecular beam. The cutoff comes earlier for larger values of z_v/z_0. The other extreme case, $(z_0/r_0)^2 \ll 1$, is when the laser beam is strongly divergent (i.e. strongly focused). The u integral is set to $1/n$ for $n < \lambda_0/(1+x^2)$ and 0 otherwise. The upper limit of the x integral will then be $x=\sqrt{\lambda_0/n-1}$ and the number of absorbed photons can be estimated as

$$I_n \propto 2z_0 e^{-(\sqrt{\lambda_0/n-1}z_0/r_0 - z_v/r_0)^2/2} \int_0^{\sqrt{\lambda_0/n-1}} dx(1+x^2)\frac{1}{n} \propto$$

$$\propto \frac{2z_0}{3} e^{-(\sqrt{\lambda_0/n-1}z_0/r_0 - z_v/r_0)^2/2} \frac{1}{n}\sqrt{\frac{\lambda_0}{n}-1}\left(2+\frac{\lambda_0}{n}\right), \quad (z_0/r_0)^2 \ll 1. \quad (5.12)$$

For intermediate values of n the expression becomes simpler:

$$I_n \propto \frac{2z_0}{3} e^{-z_v^2/2r_0^2} \lambda_0^{3/2} n^{-5/2}, \quad (z_0/r_0)^2 \ll 1, \quad 1 \ll n \ll \lambda_0. \quad (5.13)$$

A numerical evaluation of Eq. 5.9 with $z_0/r_0 = 3.0$ (almost parallel beam) is shown as triangles in Fig. 5.3. The approximation according to Eq. 5.11 is the solid line. A case with a more focused beam ($z_0/r_0 = 0.1$) is also shown in Fig. 5.3 (circles) together with the approximation of Eq. 5.12. It is obvious that the number of absorbed photons goes from a n^{-1} to a $n^{-5/2}$ distribution as the focusing of the laser increases. Further details on the theoretical model are given in Paper II.

5.2 Experimental

The calculated internal energy distribution will be compared to an internal energy distribution reconstructed from the ionic fragmentation pattern of laser excited C_{60}. The initial internal energy of excited gas phase C_{60} is the thermal energy from the oven gained in the evaporation plus the energy of the absorbed laser photons. The fullerene will then lose energy due to ionisation, fragmentation and radiative cooling. By assuming that all fragment ions are produced from C_{60}^+ and making a reasonable estimate of the decay rate for fragmentation it is possible to reconstruct the initial internal energy distribution from the fragmentation pattern observed in a time of flight mass spectrum. This approach is very similar to the one used in Chapter 7 and Paper III. The effect of energy loss due to radiative cooling will be negligible on the short time it takes for the fragment ions to be mass separated.

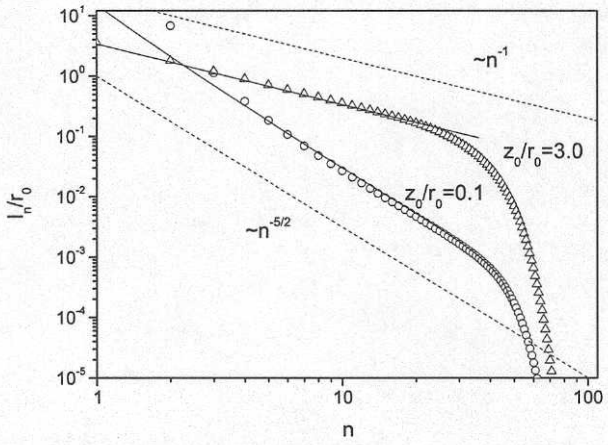

Figure 5.3: The probability to absorb n photons from a Gaussian laser beam crossed by a molecular beam for $\lambda_0 = 50$. Two limiting cases are shown $z_0/r_0 = 3.0$ (triangles) and 0.1 (circles). The approximations according to Eq. 5.11 and Eq. 5.12 are shown as solid lines. The dashed lines shows the slopes -1 and $-5/2$.

The mass spectra were obtained by heating 99.5% pure C_{60} powder to 450 – 500 °C and then exciting the C_{60} vapour with the N_2 laser (337 nm). The ions were accelerated by static electric fields in the ReToF and detected after passing two field free regions and a reflectron. The fullerene beam, the laser beam and the spectrometer axis were all perpendicular. The reflectron fields were tuned for maximum mass resolution, metastable fragmentation during the first field free region was not detected. The laser was focused by a 300 mm lens and the focal point was ~22 mm before the centre of the C_{60} beam. The fluence of the laser was changed by inserting neutral density filters in the laser beam path.

The shape (density) of the C_{60} beam was determined by evaporating C_{60} onto two glass plates in the interaction chamber. One of the plates was placed below the interaction plane of the molecular beam and the laser and the other one was placed above. It was not possible to place a plate exactly where the laser beam crossed the molecular beam but by using the results from the two plates it is straightforward to estimate the beam profile in the

interaction plane. The thickness of the C_{60} film was determined by measuring the absorption with a UV-VIS spectrometer (USB2000, Oceans Optics Inc.). To monitor the density variation of the C_{60} beam, absorption spectra were collected for points separated by 2.5 mm along a line through the center of the evaporated beam spot. The absorption peak around 430-450 nm was used as a measure of the molecular beam intensity.

The laser profile was measured by inserting a pinhole in front of a power meter and moving the pinhole across the laser beam, measuring the power for each position of the pinhole.

5.3 Results and Discussion

Time of flight mass spectra of fullerenes excited by the excimer laser, studied as a function of laser fluence, are shown in Fig. 5.4. The laser fluence ranges from 70 to 216 mJ/cm^2. It is evident that the fragmentation increases with increasing laser fluence as expected. Small, non-fullerene like fragments start appearing around a fluence of 100 mJ/cm^2. As mentioned above the fragment distribution will be used as a measure of the internal energy distribution of the excited fullerene ensemble. It is assumed that the C_{60} first ionise and then undergo sequential C_2 evaporation. C_2 evaporation will occur as long as the inverse of the fragmentation rate constant is larger than the time it takes for the ions to be mass separated, typically a few μs. The fragment distribution at the time of mass separation is the one that will be detected even if further fragmentation occurs later. It is convenient to write the fragmentation rate constant in an Arrhenius form, $k_N = A_N e^{-D_N/k_B T_e(E)}$, where A_N is the Arrhenius pre-exponential factor, D_N the dissociation energy, k_B Boltzmanns constant and $T_e(E)$ the microcanonical temperature[1]. The heat capacity is set as $C_{v,N} = (3N-7)k_B$ and $T_e(E) = (E+E_0-D_N/2)/C_{v,N}$ (the term $D_N/2$ is due to the finite heat bath correction). E_0 is the vibrational zero-point energy. The highest energy for a fullerene fragment of size N can then be obtained as follows

$$t = \frac{1}{k_N} = \frac{1}{A_N e^{-D_N/k_B T_e(E)}} \Leftrightarrow k_B T_e(E) = \frac{D_N}{\ln(At)} = \frac{D_N}{G} \Leftrightarrow$$
$$\Leftrightarrow E + E_0 - \frac{D_N}{2} = E' = \frac{D_N C_{v,N}}{k_B G}, \tag{5.14}$$

[1]For a short explanation of the concept of microcanonical temperature see Appendix A.

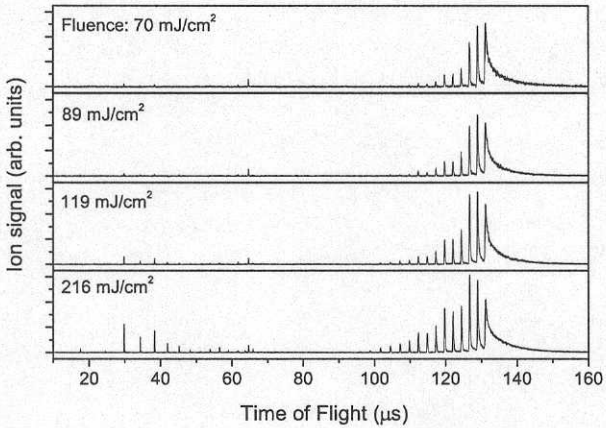

Figure 5.4: Time of flight mass spectra of C_{60} excited through multiphoton absorption from a 337 nm excimer laser at different fluences. The mass peak at 63 μs is due to pump oil.

where E' is an effective energy and G is the Gspann parameter. G will be set to 33 [8]. The width of the energy interval for fragment N will roughly be D_N so the lowest energy becomes $E_N^{min} = E_N^{max} - D_N$. The energy of interest is the energy range of the initial C_{60}^+ which decayed down to the fragment C_N^+. To get the highest energy a C_{60}^+ can have if it is going to end up as a C_N^+ one needs to add the dissociation energies it cost to reach C_N^+:

$$E_N^{max} = \frac{D_N C_{v,N}}{k_B G} + \sum_{i=N+2}^{60} D_i. \tag{5.15}$$

The upper energy limit for C_N^+ will also be the lower limit for C_{N-2}^+. The yield of fragments of size N will then be proportional to the energy interval $E_N^{max} - E_N^{min} = E_N^{max} - E_{N+2}^{max}$ times the internal energy distribution, $\rho(E)$;

$$Y_N \propto \left(D_{N+2} - \frac{D_{N+2}C_{v,N+2} - D_N C_{v,N}}{G}\right)\rho(E). \tag{5.16}$$

The difference in the energy offsets $E_0 - D_N/2$ will be rather small for the studied fragments. Thus by dividing Y_N, which can be obtained from the mass spectra, by $D_{N+2} - (D_{N+2}C_{v,N+2} - D_N C_{v,N})/G$ one can obtain an

estimate of the internal energy distribution of the excited C_{60}^+. This can then be compared to the model calculations with the appropriate parameters for laser focus, molecular beam shape etc. In the reconstruction of $\rho(E)$ from the experiments the dissociation energies from Tomita et al. [61] were used and the appearance energy of 45 eV for C_{58}^+ as E_{58}^{min} [62]. The finite heat bath correction and the zero energy E_0 are automatically included in the appearance energy.

To make an estimation of the energy distribution using the theoretical model (Section 5.1) some experimental parameters regarding the laser and the molecular beam have to be fixed. The shape of the C_{60} beam was determined by evaporating C_{60} onto two glass plates in the interaction chamber and then measuring the absorption along the plates as described in Section 5.2. The absorption data points for both the upper and the lower glass plate were plotted as a function of distance along the "center line". A Gaussian function was fitted to the points from the lower plate (since they showed the largest variations) and then the same function was fitted to the "upper" data points using only the width, r_0, as fit parameter. Assuming that the width of the molecular beam increases linearly in the direction of the beam it was possible to estimate the beam shape in the plane of the laser beam. Thus the density of the molecular beam can be described as

$$I_{mol} \propto e^{\frac{(z-z_0)^2}{2r_0^2}}, \tag{5.17}$$

where z is the distance along the direction of the beam and z_0 is the point with the maximum density. The fit gave $r_0 = 12.9$ mm. The measured data points are shown in Fig. 5.5 together with the fits and the estimated shape in the laser plane.

Regarding the focusing conditions of the laser, the beam waist, w_0, was ≤ 50 μm and the divergence, $\alpha = w_0/z_0$, was measured to 0.011 radians which gives a Rayleigh range of $z_0 = 4.5$ mm. The shot-to-shot fluctuations of the laser were on the order of 10%. These experimental conditions means that the divergent beam approximation is valid.

Fig. 5.6 shows the energy distributions (dotted lines) reconstructed from the measured mass spectra in Fig. 5.4. Together with the measured distributions are the model calculations shown as solid lines. The average absorption probability, I_n, is plotted against the internal energy $E_n = E_{th} + nE_{ph}$ with $E_{th} \sim 4$ eV and $E_{ph} = 3.68$ eV. For lower internal energies the energy distribution is proportional to $E^{-5/2}$ as expected since $z_0/r_0 = 0.35$ and thus the "divergent case" is relevant. At higher energies the cutoff becomes visible

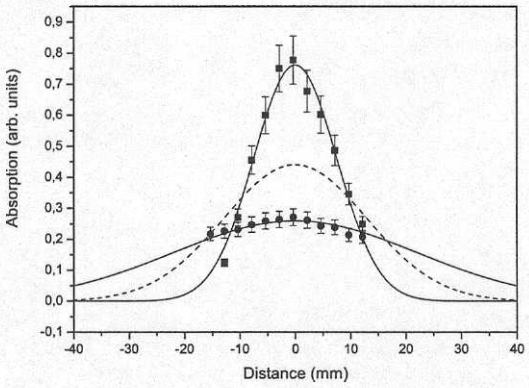

Figure 5.5: Density of the fullerene beam at two distances from the fullerene oven. The squares are before the laser interaction plane and the circles are after the laser. The points are fitted with Gaussian functions. The dashed line is an estimation of the beam density in the plane of the laser.

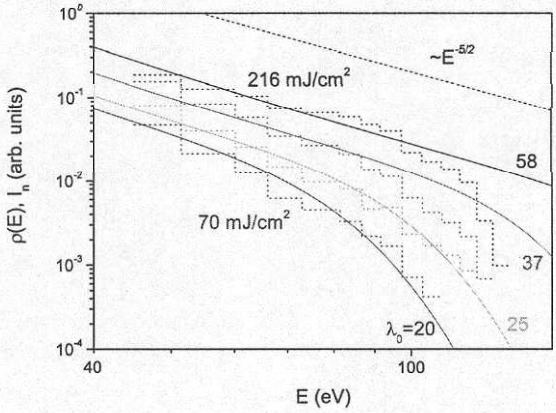

Figure 5.6: Internal energy distributions for different laser fluences acquired from the mass spectra in Fig. 5.4 (dotted lines). The solid lines are model calculations for the relevant laser and molecular beam parameters. The dashed line illustrates a slope of $-5/2$.

for the three cases with the lowest laser fluence. The agreement between experiments and model calculations are excellent with the exception of the high energy part of the two curves with the highest laser fluence where the experimental data decrease faster than the calculated curves. The faster decrease in the measurements is most likely due to the opening of a new decay channel, namely the production of small non-fullerene like fragments. In the mass spectra in Fig. 5.4 these fragments appear when the laser fluence is above 100 mJ/cm^2 and it is also these spectra that show the deviation from the calculations in Fig. 5.6. The small fragments are not produced by a sequential loss of C_2 molecules so instead it was assumed that any fullerene with an energy above a certain critical energy E_{sf} will result in small fragments.

To check the hypothesis the part of the internal energy distribution which lies above E_{sf} was integrated and compared to the total yield of small fragments observed experimentally:

$$Y_{sf} \propto \int_{E_{sf}}^{\infty} dE\rho(E) \propto \int_{\lambda_{sf}}^{\infty} dnI_n. \tag{5.18}$$

The fit parameter is the photoabsorption cross section for which $\sigma = 1.8$ Å^2 was obtained in good agreement with published values [33, 63]. From the cross section a value for the critical energy can be assigned, $E_{sf} = \sigma F_{sf} = 110 \pm 10$ eV. Fig. 5.7 shows a remarkable agreement between calculated and experimentally obtained yield of small fragments.

C_4 evaporation from the excited fullerenes, which is neglected above, could pose a problem for the modeling. This issue is shortly discussed in Paper II.

5.4 Concluding remarks

Molecules in the gas phase absorbing photons from a laser with a Gaussian profile will achieve an internal energy distribution which is not a Poisson distribution. The distribution is better described by a power law up to a certain energy where there is a cutoff. The power law ranges from E^{-1} to $E^{-5/2}$ depending on the focusing conditions and the shape of the molecular beam. The E^{-1} behaviour is typical for a parallel laser beam while a more divergent beam gives $E^{-5/2}$. Thus there is a large low energy part in the internal energy distribution which is not at all accounted for when a Poisson distribution is used to describe it. The cutoff at higher energies is fairly well

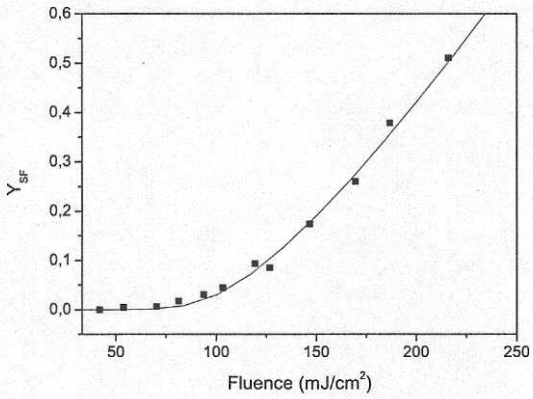

Figure 5.7: Yield of small non-fullerene like fragments as a function of laser fluence. The squares are experimental data from integrating over all small fragments in a series of mass spectra. The solid line is a calculated yield according to Eq. 5.18 (with $E_{sf} = 110$ eV).

described by a Poisson distribution though. There are ways to avoid such a broad energy distribution and one is to "trim" the laser beam to only use the center part where the intensity is fairly constant. In some experiments the low energy part is irrelevant but one should be aware of its presence.

Chapter 6

Excitation of Rydberg states in C_{60}

The excitation mechanisms behind the population of Rydberg states in C_{60} using 800 nm fs laser pulses observed in Ref. [13] are not completely determined as mentioned in Section 2.1.1. Absorption of four photons (800 nm) would supply an electronic excitation energy of 6.2 eV. This alone can not give the excitation of states covering 1-2 eV which was observed (Fig. 2.2). One possibility (based on studies of molecular Rydberg states [64]) proposed in Ref. [13] is that the vibrational energy of the C_{60} achieved in the oven, where the C_{60} is heated to 500 °C to come into the gas phase, can be used by the electrons to populate the states with an energy higher than 6.4 eV. The electrons are initially excited near the core where the electronic and vibrational states are mixed for intermediate Rydberg states and where neither the Born-Oppenheimer nor the inverse Born-Oppenheimer approximation holds. In this mixed region the electrons could get extra energy from vibrations needed to cover higher states (or deposit energy in the vibrational states). Once the electrons move away from the core in their Rydberg orbital the electronic and vibrational states become decoupled. The core energy is thus conserved and discrete peaks are seen in the photoelectron spectra. Molecules that are ionised without populating Rydberg states will contribute to the broad, unresolved underlying peak observed in the electron spectra.

There are more potential explanations, e.g. Ref. [65], and further experiments are necessary. One important part in the further investigations of the excitation mechanisms would be to study vibrationally cold fullerenes. If the possible coupling between electronic and vibrational excitation is important it would affect the possibility of exciting Rydberg states in cold C_{60}.

6.1 Experimental

To set up an experiment probing the importance of vibrational energy in the excitation of Rydberg states the previously described Cold Source was moved from Göteborg to the Max-Born-Institute in Berlin and combined with the electron/ion spectrometer and fs lasers there. The Cold Source was connected to the interaction chamber of the ReToF so that the molecular beam from the Cold Source enters perpendicular to the axis of the ion and electron spectrometers. On the opposite side from the Cold Source an effusive oven was mounted horizontally, parallel to the cold molecular beam and perpendicular to the spectrometer axis. The laser light was guided in vertically from the top of the chamber in order to be at right angles with both the molecular beam and the spectrometer axis. A schematic view of the configuration is shown in Fig. 6.1. Commercial C_{60} (99.4% purity) was

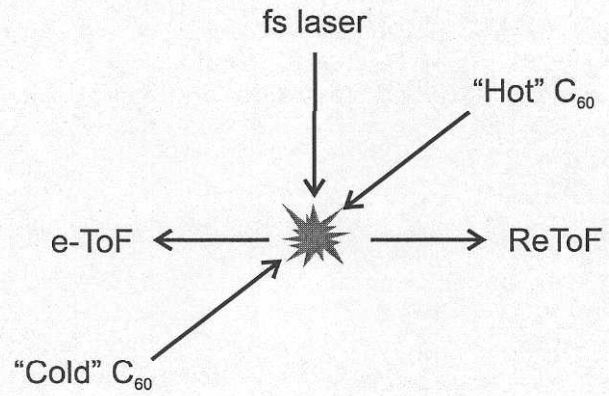

Figure 6.1: C_{60} from either an effusive oven or a vibrationally cold molecular beam is excited by a femtosecond laser coming in from the top of the vacuum chamber at right angles with the C_{60} beams. The created ions or photoelectrons can be extracted and detected orthogonally to the laser and C_{60} beams.

used both in the "normal" effusive oven and the effusive oven in the Cold Source. Both ion mass spectra and photoelectron spectra were collected from the "hot" oven first for some different laser fluences. This was to ensure that it was possible to observe the Rydberg states and to get some characteristics from the fragmentation pattern. Only 800 nm photons were used and the pulse length was always 100 fs, the fluence was typically varied between 0.1 J/cm^2 and 7 J/cm^2. Immediately after these measurements the Cold Source

was activated and the hot oven turned off, keeping the conditions as similar as possible. The experiments were repeated using the vibrationally cold C_{60}. Both the laser fluence and the electron spectrometer were calibrated using Xe [66].

A gas aggregation source like the Cold Source can not merely produce vibrationally cold fullerenes but also clusters of fullerenes if the density of the fullerene vapour is high enough as mentioned in Section 3.2. The presence of clusters of fullerenes would be a clear indication that the fullerenes coming from the Cold Source really are vibrationally cold. On the other hand it is not desirable to have clusters present in the cold fullerene beam while doing experiments on Rydberg electrons. Therefore the temperature of the oven in the Cold Source must not be so high that the density of the fullerene vapour is high enough to create clusters. This means that by turning up the oven temperature from "normal" working temperature one should be able to observe clusters of fullerenes and they should disappear again once the temperature is lowered. Such a behaviour would indicate that the fullerenes really are cold, and that the experiments are done under the correct conditions. However, there are some experimental difficulties with detecting the clusters. Laser light with a photon energy lower than the ionisation potential of C_{60} tends to heat and break up the clusters rather than just ionising them which makes the detection efficiency rather poor.

In order to look for clusters the MCP detectors in the mass spectrometer were floated up to ~6 kV to increase the sensitivity. The checks were done using the spectrometer as a linear ToF mass spectrometer. The temperature of the oven in the Cold Source was varied from normal working conditions to higher temperatures where clusters could be expected to form and then it was lowered again. Different floating of the MCP:s was also employed.

6.2 Results and Discussion

A mass spectrum of C_{60} ionised with an 800 nm 100 fs laser normally shows fragmentation and singly, doubly and sometimes triply charged C_{60}. One such spectrum obtained at a laser fluence of 0.3 J/cm^2 (oven temperature 450 °C) is shown in Fig. 6.2 (a). The peaks from C_{60}^+ and C_{60}^{++} are almost of the same size and there is a smaller peak due to triply charged C_{60}. Some minor fragmentation (prompt and metastable) is present. A spectrum of the photoelectrons created under very similar conditions (laser fluence 0.3

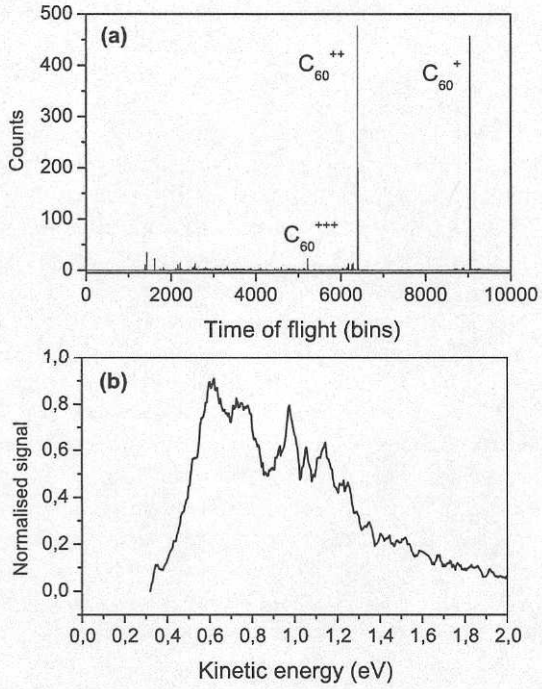

Figure 6.2: Spectra obtained with an 800 nm 100 fs laser with a fluence of 0.3 J/cm^2. **(a)** Time of flight mass spectrum of C_{60}. **(b)** Photoelectron spectrum from C_{60} evaporated at 530 °C. Peaks from electrons ionised from Rydberg states can be seen between 0.7 and 1.3 eV.

J/cm^2, oven temperature 530 °C) is shown in Fig. 6.2 (b). Structure due to electrons from Rydberg states can be clearly seen between 0.7 and 1.3 eV. The Rydberg peaks are not so nicely resolved as some of the peaks in Fig. 2.2 but those were produced using another laser system with a longer pulse duration.

Switching from a hot effusive C_{60} source to the beam of vibrationally cold (liq. N_2 temp.) C_{60} coming from the Cold Source naturally results in a lower density of C_{60} and a lower count rate but still it is no problem getting decent ion spectra. A mass spectrum from the Cold Source obtained at a laser fluence of 0.3 J/cm^2 and an oven temperature of 450 °C is given in Fig. 6.3

(a). When working with the Cold Source the accelerated C_{60} ions need to be deflected more than the ions from the hot oven in order to reach the detector. This is due to the finite velocity perpendicular to the spectrometer axis that the cold C_{60} have from the Cold Source, which is higher than the C_{60} coming from the oven. There is relatively more background signal present in the cold C_{60} spectra. This is partly an effect of the lower C_{60} density which makes the C_{60} signal look smaller compared to the ever present background but there is also some additional oil peaks coming from the diffusion pump pumping the Cold Source. Some smaller C_{60} fragments are also present.

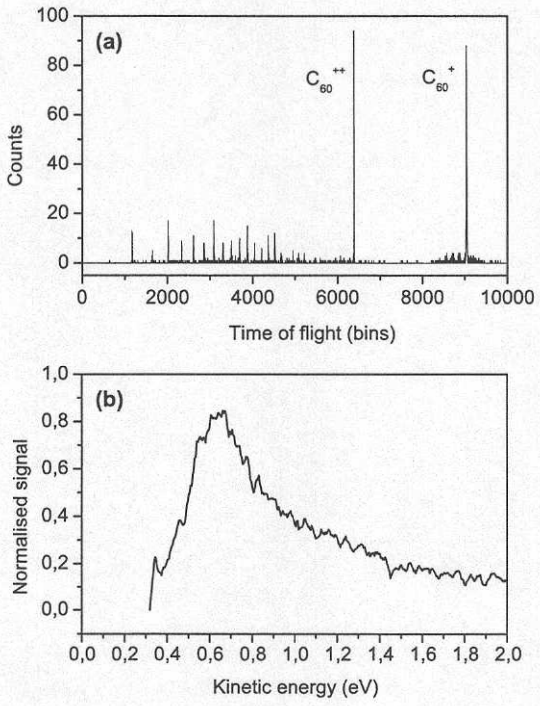

Figure 6.3: Spectra from vibrationally cold C_{60} obtained with an 800 nm 100 fs laser with a fluence of 0.3 J/cm^2. **(a)** Time of flight mass spectrum of C_{60}. **(b)** Photoelectron spectrum from cold C_{60}. Only a thermal electron distribution without Rydberg peaks is present.

A photoelectron spectrum of C_{60} from the Cold Source is displayed in Fig. 6.3 (b). The laser fluence was 0.3 J/cm^2 and the fullerenes were evaporated at 440 °C.

The difference between Fig. 6.3 (b) and the spectrum of vibrationally hot C_{60} in Fig. 6.2 (b) is striking. The "cold" electron spectrum looks like a thermal electron distribution (from hot electrons, heated by the laser) as seen in Ref. [7] and shows no Rydberg peaks. Electron spectra of C_{60} from the hot effusive oven and the Cold Source were compared for a large variety of Cold Source oven temperatures (440 – 512 °C) and laser fluences (0.1 – 7 J/cm^2) always without observing any Rydberg peaks in the Cold Source spectra. The vibrational temperature of the C_{60} from the Cold Source is always expected to correspond to liq. N_2 temperatures. Increasing the oven temperature merely serves to increase the density. A comparison of "hot" and "cold" electron spectra is shown in Fig. 6.4. These results are in agreement

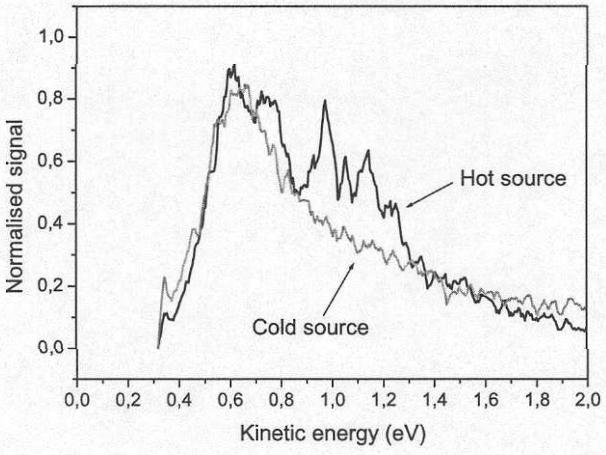

Figure 6.4: Typical photoelectron spectra of C_{60} from the "hot" effusive oven and the Cold Source, obtained with an 800 nm 100 fs laser at a fluence of ca. 0.3 J/cm^2. The hot oven was at 530 °C and the oven in the Cold Source at 440 °C. Note that the oven temperature in the Cold Source merely serves to evaporate the fullerenes, their vibrational temperature after the quenching is lower than 100 K. There are clear Rydberg peaks present in the "hot" spectrum while the "cold" spectrum only shows thermal electrons.

with what is predicted by the model proposed for the excitation mechanism of Rydberg states in Ref. [13].

When the mass spectrometer was set up to detect possible clusters of fullerenes, $(C_{60})_N$, no signs of clusters were seen at normal temperatures of the Cold Source oven (~450 °C). As the temperature was increased (and thereby the density of the C_{60} vapour) signs of heavier species started to appear in the mass spectra as shown in Fig. 6.5. If the temperature is turned back

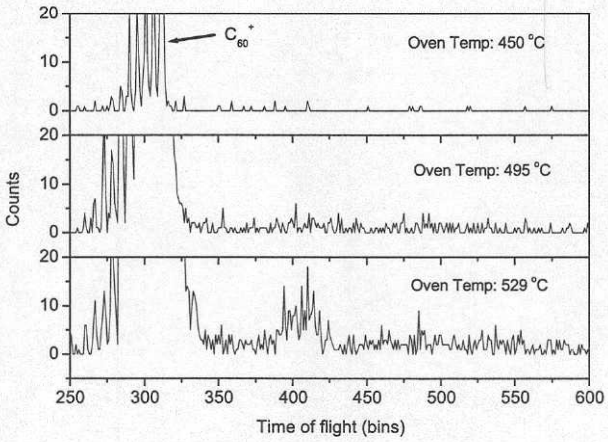

Figure 6.5: Mass spectra zoomed in at the range of C_{60}^+ and higher masses. The spectrometer is optimized to detect clusters of fullerenes. At lower oven temperatures (450 and 495 °C) C_{60}^+ is the heaviest mass while at 529 °C heavier species starts to appear.

down again these heavy species disappear. This is a clear indication that the correct experimental conditions were used, as discussed above. Structures roughly corresponding to $(C_{60})_2^+$ and $(C_{60})_3^+$ are seen in Fig. 6.6. However, these structures show some unexpected and interesting features. They seem to consist of a distribution of peaks separated by C_2 masses. This is different from the situation when a F_2 laser is used to one-photon ionise clusters of fullerenes [40, 41]. C_2 evaporation from C_{60} dimers and trimers is very surprising. This unexpected behaviour is further investigated in Chapter 8.

Additional two colour pump-probe experiments with the hot source have been

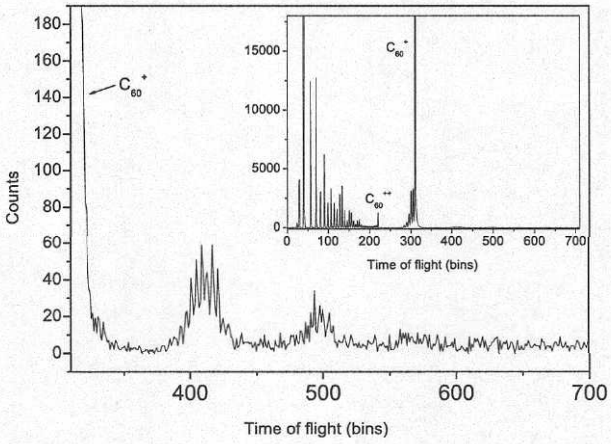

Figure 6.6: Mass spectrum from the Cold Source obtained at an oven temperature > 500 °C zoomed in on the region of masses higher than C_{60}. There seems to be two distributions of peaks separated by C_2 units as coming from fragmentation of $(C_{60})_2$ and $(C_{60})_3$. The inset shows the entire mass spectrum.

performed by M. Boyle where one weak blue (400 nm) fs laser pulse and a stronger red (800 nm) pulse was used. When there is an overlap between the two pulses and when the red follows the blue the intensity of the Rydberg peaks is enhanced 3-5 times. This, along with other observations, has been interpreted such that the blue pulse pre-excites the (LUMO+1) state which is considered as a doorway state for excitation of Rydberg states [67, 68]. The blue pulse is nearly resonant with the doorway state while it takes two red pulses to excite it. A strong population of the (LUMO+1) state has been observed in theoretical work where fs laser excitation of C_{60} was modeled using a density-matrix formalism and considering the strong electric field of the laser [69]. The theoretical calculations also predicted that there would be an oscillatory exchange of energy between the lattice and the excited electrons on the order of 2 eV (assigned as the A_g breathing mode). This exchange could give rise to the broad population of Rydberg states. If the fullerenes are vibrationally cold the lowest excited vibrational mode would only be populated to 0.6% and very little vibrational motion can couple to the excited electrons explaining why no Rydberg states are observed.

The excitation mechanisms of the Rydberg states are quite nicely explained in Refs. [67, 68] but some additional work could be done to further clarify the processes. The first thing would be to do pump probe experiments where the wavelength of the pump is varied to check how sensitive the excitation of a "doorway state" is to pump colour and compare the results to the calculations in Ref. [69]. Another interesting subject is how the population of Rydberg states depend on vibrational energy in more detail. Vibrationally cold C_{60} can be heated to a specific temperature using a heating cell made out of copper placed after the aggregation chamber, as described in Ref. [70]. Possibly such experiments could clarify whether the excitation of Rydberg states scales with the population of vibrational states.

6.3 Concluding remarks

To excite Rydberg states in C_{60} by 400 and 800 nm fs laser pulses an initial internal vibrational energy of the fullerenes is necessary. The excitation mechanisms can be described in terms of multielectron excitation of a doorway state. In the doorway state there is a coupling to vibrational energy broadening the state in energy and from this doorway state the Rydberg states are excited. If the fullerenes are vibrationally cold this coupling does not take place and the broad range of Rydberg states are not excited. However, other explanations are plausible and further experimental and theoretical work on this topic would be desirable.

Chapter 7

Radiative cooling of fullerenes and endohedral fullerenes

Photon emission from laser excited fullerenes in a vacuum chamber is difficult to detect directly. Nevertheless it is important in the competition between different decay channels of highly excited fullerenes as mentioned in Section 2.1. An accurate description of the radiative energy loss is crucial for a reliable modeling of the dynamics of excited fullerenes. The experimental difficulties can be got around by for example studying the metastable fragmentation of fullerene ions in a reflectron time of flight mass spectrometer. By doing this it is possible to learn things about the radiative energy loss and the emissivity[1] of the ions. The technique was employed for the first time on fullerenes by Hansen and Campbell in 1996 [24]. The idea is to study the metastable fragmentation which occurs during the first field free region of the mass spectrometer. Metastable fragmentation is here regarded as fragmentation which takes place after the time when the ions have become mass separated and before they enter the reflectron. Fragmentation occurring before mass separation is named prompt fragmentation. The metastable fragmentation ratio (the fraction of ions that fragments metastable divided by the sum of the metastable and the prompt fragments) depends strongly on the internal energy of the ions. Excited fullerenes will all the time lose energy due to radiation so by changing the time between the exciting laser pulse and the extraction of ions in the mass spectrometer it is possible to vary the cooling time for the ions before they enter the metastable fragmentation window. One can thus, in a rather controlled way, vary the internal

[1]The emissivity is defined as the radiated power divided by the power radiated by a black body radiator at the same temperature according to Stefan-Boltzmanns law.

energy of the fullerenes that fragment metastable. Comparing the experimentally measured metastable fragmentation ratio to a theoretical estimate (explained later) can give values for the emissivity.
Radiative cooling from fullerenes has been studied in many ways since 1996, both theoretically and experimentally, see e.g. Refs. [26, 27, 71–73]. Here the experiments are expanded to include fullerenes from C_{46} to C_{82}. The radiative behaviour of endohedral fullerene ($La@C_{82}$) fragments is also investigated and compared to the empty fullerenes.

7.1 Experimental

The experimental method was the same as in Ref. [24] with the major difference that the N_2 laser was used instead of a more powerful XeCl laser as in 1996. The samples studied were commercially purchased C_{60} and C_{70} (purity of 99.8% and 98+%, respectively), C_{84} derived from fullerene soot by HPLC and $La@C_{82}$ produced by arc discharge [4, 29]. The fullerene powder was heated to $480-580$ °C and the vapour was excited by a focused N_2 laser as mentioned above. The laser fluence was typically around 200 mJ/cm^2. The ions were accelerated from the ionisation region by pulsed extraction fields with a time delay with respect to the laser pulse. Changing this delay changes the cooling time of the fullerenes. The fields in the reflectron were set to place the metastable fragment almost exactly between the prompt peaks for best resolution. An ion which starts its flight as C_N^+ and then decays to C_{N-2}^+ during the first field free region will arrive at the detector before the mother C_N^+. Dividing the area of the metastable peak by the total area of the metastable and the prompt peak will then give the metastable fraction of the specific fullerene.

7.2 Theoretical modeling

The description of the theoretical approach done here closely follows the derivation in Ref. [24] with a few exceptions and improvements. A slightly different approach (possibly more understandable) is used in Paper III and Appendix B.

Within the framework of the evaporative ensemble [74, 75] it is possible to define a highest and a lowest temperature for isolated clusters at a certain

time after their excitation, similar to the approach in Section 5.3. There is a highest temperature because if the cluster would have had more energy it would decay to one size smaller and in the same way there is a smallest temperature since clusters with a lower energy would not have fragmented from the larger size. Inherent in this discussion is that all clusters have undergone at least one fragmentation. If only cooling through fragmentation is considered the highest energy (crossover energy E_c) for a cluster of size N at time t can be defined as

$$E_c(t) = C_v(N)T(t) - E_0(N) \approx C_v(N)\frac{D_N}{G(t)k_B} - E_0(N) \qquad (7.1)$$

where C_v is the heat capacity, T the temperature, D_N the dissociation energy, G the Gspann parameter and $E_0(N)$ represents the deviation from constant heat capacity for size N. The temperature T is the microcanonical temperature with the finite heat bath correction so that $T = T_{MC} - D_N/2C_v$ where T_{MC} is the microcanonical temperature. A short explanation of the concept microcanonical temperature can be found in Appendix A. The temperature is given as $T \approx D_N/Gk_B$.[2] If the heat capacity and the energy offset E_0 scales linearly with N the terms involving differences of these quantities can be ignored and the width of the energy distribution for size N will be proportional to

$$I_N \propto C_v\frac{D_N}{Gk_B} - \left(C_v\frac{D_{N+2}}{Gk_B} - D_N\right) = D_N - \frac{C_v}{Gk_B}\left(D_{N+2} - D_N\right) \qquad (7.2)$$

where C_v is the common heat capacity. If there is a sufficiently smooth initial energy distribution this width will also be proportional to the amount of particles of size N.

Once the fragment ions in a time of flight mass spectrometer have been mass separated the number of clusters in the ion bunch with size N will only decrease. There will be no addition from ions fragmenting from size $N+2$ in the field free region since they will end up in a metastable peak, but there will be a loss due to metastable fragmentation from size N to $N-2$ which will also end up in a metastable peak. This means that during the flight through the spectrometer the lower limit of the energy distribution for size N will not change while the upper one will, due to metastable fragmentation. Naming the time when mass separation is achieved t_1 and the time when the ions enter the reflectron t_2 (which marks the end of the time window for metastable

[2]Assuming that there is a 1/t decay (as the case for an ensemble with a broad energy distribution) one can write $k = 1/t = Ae^{-D_N/k_BT} \Leftrightarrow D_N/k_BT = \ln(At) = G$, where A is the Arrhenius pre-exponential factor [25].

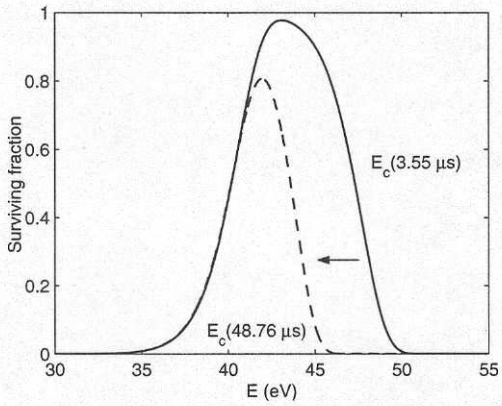

Figure 7.1: Calculated internal energy distributions for C_{50}^{+} at times $t_1 = 3.55$ μs and $t_2 = 48.76$ μs. The part in between the right flank of the dashed and the solid line is the fraction that will decay during the first field free flight and thus end up in a metastable peak in the mass spectrum. The dissociation energy is set to 8.8 eV, the Arrhenius pre-exponential factor to $2{\cdot}10^{19}$ s^{-1} and $E_0 = 7.04$ eV.

fragmentation), the crossover energy will move from $E_c(t_1)$ to $E_c(t_2)$ during this time interval. This is illustrated in Fig. 7.1. The energy interval for metastable decay (or the width of the metastable energy distribution) will be

$$E_c(t_1) - E_c(t_2) = \frac{C_v D_N}{k_B}\left(\frac{1}{G(t_1)} - \frac{1}{G(t_2)}\right) \approx \frac{C_v D_N}{k_B}\frac{\ln(t_2/t_1)}{G(\bar{t})^2} \tag{7.3}$$

where $\bar{t}$ is the geometric average of t_1 and t_2.

Dividing this by the width of the initial energy distribution for size N (Eq. 7.2) gives

$$\frac{E_c(t_1) - E_c(t_2)}{I_N} \propto \frac{\frac{C_v D_N}{k_B}\frac{\ln(t_2/t_1)}{\overline{G}^2}}{D_N - \frac{C}{G(t_1)k_B}(D_{N+2} - D_N)}. \tag{7.4}$$

If $D_N \approx D_{N+2}$ then one can write the metastable fragmentation probability without any radiative cooling as

$$p \approx \frac{C_v}{\overline{G}^2 k_B}\ln(t_2/t_1). \tag{7.5}$$

This relation says that if radiative cooling is a negligible effect and G can be considered constant on the relevant timescale, plotting the experimentally measured metastable fragmentation ratio as a function of $\ln(t_2/t_1)$ would render a straight line going through the origin. As shown in Ref. [24] the experimental data gave a straight line but it did not go through the origin. For a reasonable analysis radiative cooling has to be taken into account.

Radiative cooling will reduce the internal energy like

$$\left(\frac{dE}{dT}\right)_{rad} = -\varepsilon\sigma_{SB}ST_{Rad}^4 \tag{7.6}$$

where ε is the emissivity, σ_{SB} is the Stefan-Boltzmann constant, S the surface area of the cluster and T_{Rad} the temperature. The microcanonical temperature T_{Rad} has a different finite heat bath correction than the "evaporative" microcanonical temperature T as explained in Appendix A. T_{Rad} is equal to $T_{MC} - h\nu/2C_v$ but here the correction will be ignored since it is small compared to $D/2C_v$. T_{Rad} will be written in terms of the evaporative temperature like $T_{Rad} = T + D_N/2C_v$. This is different from Ref. [24] where $T_{Rad} = T$ was used.

Considering the energy loss due to radiative cooling and following the derivation described in the appendix of Ref. [24] one can arrive at the following ratio of metastable fragmentation[3]

$$p \approx \frac{C_v}{\overline{G}^2 k_B}\left(\ln(t_2/t_1) + \ln[(1-e^{-\Delta})/\Delta]\right) \tag{7.7}$$

where the radiative cooling is responsible for the term Δ which is

$$\Delta = \frac{\varphi}{(t_2 - t_1)} = \frac{D_N^3 \varepsilon_N \sigma_{SB} S_N}{(t_2 - t_1)\overline{G}^2 k_B^3 C_v}\left(1 + \frac{G}{2C_v}\right)^4, \tag{7.8}$$

where the last term is the correction due to the different finite heat bath corrections to the temperatures.

[3]In Ref. [24] the evaporation probability was given as

$$p \approx \frac{C_v}{G^2 k_B}\ln(t_2/t_1) + \ln[(1-e^{-\Delta})/\Delta] - \Delta.$$

However, the last Δ should not be included, it appeared due to the erroneous inclusion of the term $(dE/dt)_{rad}$ in Eq. (A4) in Ref. [24].

A more explicit derivation of Eq. 7.7 and Eq. 7.8 following Paper III can be found in Appendix B.

Eq. 7.7 says that if the experimental metastable ratio is to be plotted as a function of $\ln(t_2/t_1)$ it will give a straight line just as also Eq. 7.5 says, but with a negative intercept of the y-axis due to the extra term $\ln[(1-e^{-\Delta})/\Delta]$ which comes from the radiative cooling effect. From such a plot it would thus be possible to extract an estimate for Δ and, indirectly, ε.

7.3 Results and Discussion

Two typical mass spectra from the experiments on radiative cooling are shown in Fig. 7.2. They are obtained with two different delays on the extraction and one can clearly see that the relative amount of metastable fragmentation is lower for the longer delay. The metastable fraction was estimated

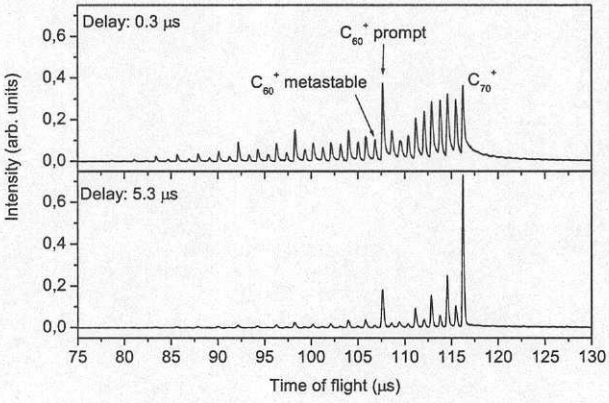

Figure 7.2: Time of flight mass spectra of C_{70} with two different delays on the extraction.

by integrating the fragment peaks and then dividing the metastable peak area by the sum of the metastable peak and its parent. Since there is a background in the spectra due to delayed ionisation, fragmentation during the

initial acceleration and an electrical offset a background adjustment had to be made. For simplicity (and consistency with Ref. [24]) the lowest points between the peaks were identified and connected by straight lines. These lines were then used as baselines for the integrations. One data set for a specific starting material (C_{60}, C_{70}, C_{84} or La@C_{82}) consisted of mass spectra with extraction delay times of 0.3, 0.8, 1.3 and so on up to 7.3 μs. The upper limit was determined by loss of signal for the smaller fragments. For each delay time typically $3-5$ spectra were collected. For every starting sample there are at least 3 data sets. All fragment peaks were integrated and then the metastable fraction (p) was calculated and plotted as a function of $\ln(t_2/t_1)$ as seen in Fig. 7.3. The times t_1 and t_2 (the time for mass separation and

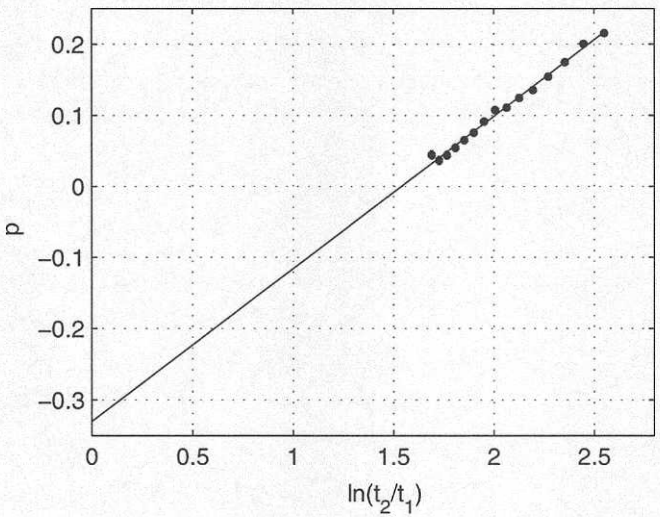

Figure 7.3: Metastable fractions of C_{60}^+ as a function of $\ln(t_2/t_1)$. The straight line is a linear fit of the data. See text for further details.

entrance of the reflectron respectively) were calculated by using the applied extraction and reflection fields and the dimensions of the spectrometer. A straight line was fitted to the data points. The fit can be compared to Eq. 7.7 and a value for Δ can be extracted. The fits were weighted by the errors for the individual data points so that a point with a large error will be less influential on the fit. In the present case the samples are rather few $(3-5)$ so there is a certain risk that some sample points just happen to lie close giving a data point an unrealistically small error. This data point will then

get a too high weight in the fit. To avoid the problem it was assumed that the errors become larger with smaller fragment sizes and the errors were estimated by a linear fit of σ_N as a function of N. These errors were then used in the fitting procedure. Naturally all fits had to be checked so that they did not become unrealistic due to data points lying way off.

If the fitted line is written like $p_{fit} = a\ln(t_2/t_1) + b$ then Eq. 7.7 yields

$$b/a = \ln[(1 - e^{-\Delta})/\Delta]. \tag{7.9}$$

Eq. 7.9 can then be solved numerically for Δ. The error in Δ was assumed to be $\sigma = \sqrt{(\delta a/a)^2 + (\delta b/b)^2}$, where δa and δb are the errors in a and b obtained from the fit. This is actually a slight overestimation of the error.

As described in Paper III the data has to be adjusted since the internal energy distribution of the fullerenes is not as flat as assumed in the theoretical modeling. The internal energy distributions in the present experiments are more likely to be of the form

$$\rho(E) = ce^{-\alpha E} \tag{7.10}$$

where ρ is the energy distribution, E is the energy and c and α are constants. Using the same reasoning as in Paper II and Section 5.3 the value for α for the different starting fullerenes can be fitted from the mass spectra.

As mentioned above there are at least three data sets for each starting material. The weighted average of these was calculated according to

$$\overline{\Delta} = \frac{\sum_i \Delta_i/\sigma_i^2}{\sum_i 1/\sigma_i^2} \tag{7.11}$$

where σ_i is the error estimation of Δ_i and the i's denotes the different sets. The errors of the mean values from Eq. 7.11 are set as

$$\sigma^2 = \Big(\sum_i \frac{1}{\sigma_i^2}\Big)^{-1}. \tag{7.12}$$

The parameter that is measured in these experiments is εD_N^3. To extract εD_N^3 from Eq. 7.8 the value of a few variables needs to be fixed. $\overline{G}$ is set to 31, $C_v = (3N - 6)k_B$ and the area S_N is calculated using the molecular radius of C_{60} and then scaling with the number of atoms, all to be consistent with Ref. [24].

Fig. 7.4 shows a comparison of the present results for εD^3 for C_{60}^+ fragments and the ones obtained in Ref. [24]. The results from Ref. [24] have been corrected for the extra Δ that appeared in that paper and for the finite heat bath correction due to the different temperatures as discussed in Section 7.2. As can be seen the agreement is very good so there is a reproducibility of the results even though a different laser has been used. In Fig. 7.5 experi-

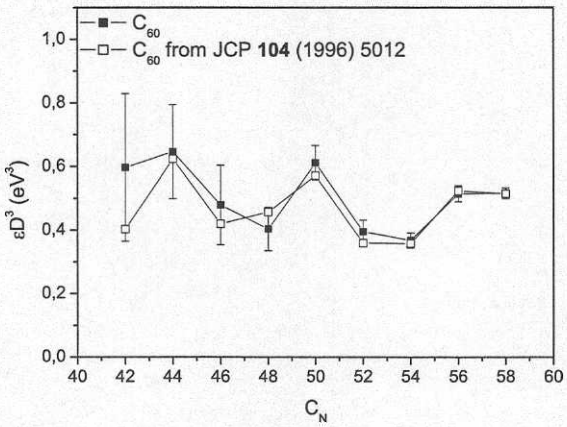

Figure 7.4: Emissivity times dissociation energy cubed for fragments of C_{60}^+ from the present experiments (full squares) compared to results from Ref. [24] (open squares).

mental values of εD^3 are shown for the ionic fragments of C_{60}, C_{70} and C_{84}. For some fragments (i.e. C_{52}^+ - C_{56}^+) there is a small difference in the values depending on the starting material. This could be due to the fact that the signal intensity for the species that have fragmented many times naturally becomes smaller so that the data for these become more uncertain. However, the small difference could also be an effect of neutral fragmentation. In the theoretical modeling it is assumed that the fullerenes first ionise and then fragment sequentially. A certain fragment size will correspond to a certain part (with the approximate width D) of the initial internal energy distribution of the entire ensemble. The neutral dissociation energies are different from the charged (approx. 0.5 eV higher [18]) so if a fullerene fragments for example five times and then ionises it will not have the same energy as a fullerene which first ionises and then fragments five times. The contribution

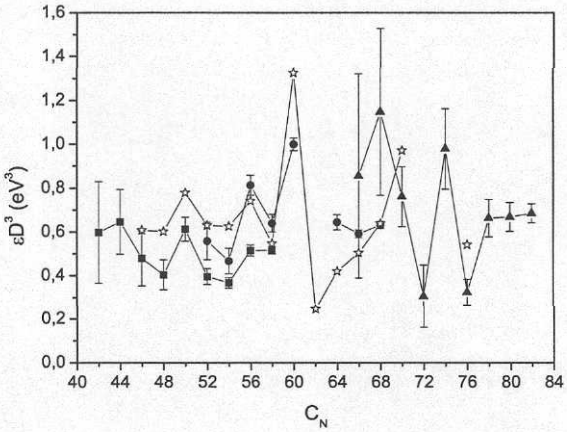

Figure 7.5: Emissivity times dissociation energy cubed for fragments of C_{60}^+ (squares), C_{70}^+ (circles) and C_{84}^+ (triangles). The open stars are values reconstructed from Ref. [61]. See text for more details.

to the mass spectra from the neutral channel will be most significant for the species that only fragment a few times, thus these are the ones that would be most distorted by the effect. Values for C_{62}^+ are missing in the plot since the theory is not quite valid for that molecule due to the low dissociation energy which gives a narrow internal energy distribution meaning that the "edges" of the distribution not are well separated as assumed in the theory.

The present data can be compared to results from Aarhus where a similar experimental approach was used [61]. In that paper εD^3 was also measured and the emissivity ε was calculated using the theoretical model described in Ref. [71]. It was then possible to get an estimation of the C_2 dissociation energies for the studied fullerenes. In Ref. [61] it is predicted that the emitted power for C_{60}^+ is 33000 eV/s at 3000 K and that the power is proportional to the number of atoms and to the temperature to the power of six. The emissivity for C_{60}^+ can thus be written as

$$\varepsilon = \frac{P}{S\sigma_{SB}T_{Rad}^4} = \frac{cT_{Rad}^6}{S\sigma_{SB}T_{Rad}^4} \approx \frac{c}{S\sigma_{SB}}\left(\frac{D}{Gk_B} + \frac{D}{2C_v}\right)^2 \tag{7.13}$$

where P is the emitted power, S the surface area of the fullerene, T_{Rad} temperature, D the dissociation energy, G the Gspann parameter and c a proportionality constant. c was found to be $4.5{\cdot}10^{-17}$ eV/K^{6}s. The radiated power scales with the number of atoms but so does the surface area S so ε is independent of this. By using the dissociation energies published in Ref. [61] in Eq. 7.13 and multiplying the obtained ε's with D^3 it should be possible to reconstruct the values of εD^3 measured in Ref. [61] even though they are not given explicitly in the paper. The values are plotted as open stars in Fig. 7.5 for comparison. The agreement with the results presented here is fair, especially considering that the results are obtained in different ways with different equipment.

Fig. 7.6 shows a comparison of εD^3 for C_N^+ and La@C_N^+. The values are more or less the same for C_N^+ and La@C_N^+ considering the accuracy of the experiments. The dissociation energies for La@C_N^+ are not well known so the

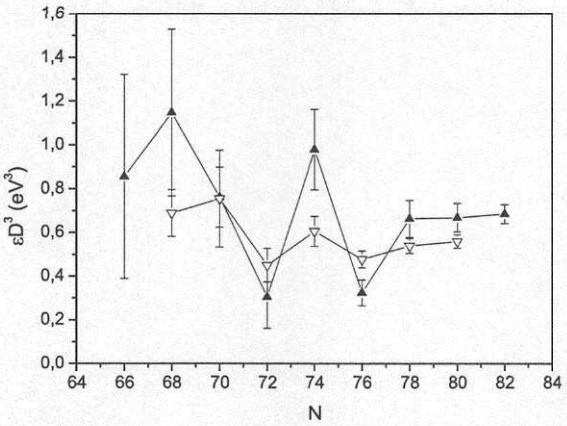

Figure 7.6: Values of εD^3 for C_N^+ (filled triangles) and for La@C_N^+ (open triangles).

fact that C_N^+ and La@C_N^+ have similar values for εD^3 does not necessarily mean that they have the same radiation behaviour. However, measurements done on La@C_{84}^+ have shown that the binding energies of C_{80}^+ and La@C_{80}^+ are equal (within the experimental errors) [76] so it seems reasonable to assume

that the confinement of a lanthanum atom inside the fullerene does not alter the radiation behaviour considerably.

Emissivity

The quantity measured for the fullerenes in the present experiments is the emissivity times the dissociation energy cubed. The interesting part, however, is the radiation (unless one considers the emissivity the best known quantity and wants to estimate the dissociation energy like in Ref. [61]). Assuming that the dissociation energies for the relevant fullerenes are known the emissivities can be extracted. C_2 binding energies for fullerenes have been discussed for many years as mentioned in Chapter 2 so there are several different values published. Here the relative dissociation energies measured by Barran et al. are used normalised to 10.1 eV for C_{60}^+ which is one of the most recent values [23]. Emissivities obtained using those values are displayed in Fig. 7.7. The open stars in Fig. 7.7 are the theoretical emissivities

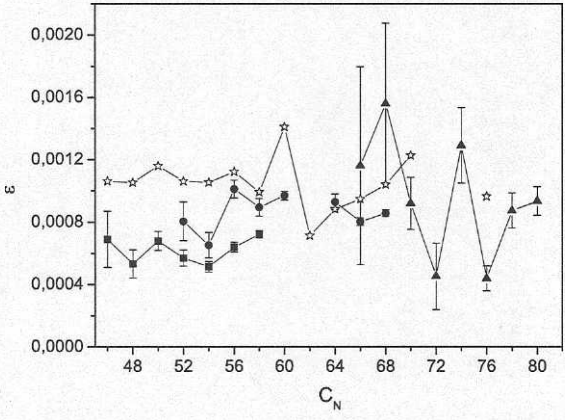

Figure 7.7: Measured emissivities for ionic fragments of C_{60} (squares), C_{70} (circles) and C_{84} (triangles). The open stars are calculated emissivities from Ref. [61].

from Ref. [61] obtained from Eq. 7.13 as described above.

As previously mentioned the emissivity from clusters can also be estimated theoretically. From detailed balance one can write a rate for photon emission from a cluster

$$k(E,\omega)d\omega = \frac{\omega}{h\pi^2c^2}\sigma(E-\hbar\omega,\omega)\frac{\rho(E-\hbar\omega)}{\rho(E)}d\omega \tag{7.14}$$

where ω is the angular frequency of the photon, c the speed of light, σ the photoabsorption cross section, ρ the density of states and E is the energy of the cluster [12, 61, 74]. When photo absorption cross sections are measured the experimental results normally also include a term due to the stimulated emission of photons which gives an over all reduction of the cross section. Under the assumption that the cross section is independent of energy so that $\sigma(E-\hbar\omega,\omega) = \sigma(E-2\hbar\omega,\omega)$ the measured cross section will be

$$\sigma_{meas}(\omega) = \sigma(\omega)\left(1-\frac{\rho(E-2\hbar\omega)}{\rho(E-\hbar\omega)}\right). \tag{7.15}$$

By also approximating the ratio of level densities by $\rho(E-2\hbar\omega)/\rho(E-\hbar\omega) \approx \exp[-\hbar\omega/T_{Rad}(E-3\hbar\omega)]$ and saying that the cluster temperature T_{Rad} is independent of a change of energy on the order of $\hbar\omega$ it is possible to write the rate of photon emission from the cluster as

$$k(E,\omega) = \frac{\omega^2}{\pi^2c^2}\sigma(\omega)\frac{1}{e^{\frac{\hbar\omega}{k_BT}}-1}d\omega. \tag{7.16}$$

Further details are given in Refs. [12, 71, 74].

The most problematic part in Eq. (7.16) is the photoabsorption cross section. Metal clusters in the free electron model approximated as small metal spheres offers a relatively simple expression for the the cross section;

$$\sigma = \frac{q^2}{m_ec\epsilon_0}\gamma N_e\frac{\omega^2}{(\omega^2-\omega_s^2)^2+(\gamma\omega)^2} \tag{7.17}$$

where q is the elementary charge, m_e is the electron mass, c is the speed of light, ϵ_0 the dielectric constant, N_e the number of valence electrons and ω_s is the frequency of the surface plasmon resonance [12, 71, 77, 78]. The width of the resonance peak is γ. Putting Eqs. (7.16) and (7.17) together gives a fairly easy to use model for photon emission from metal clusters provided that the surface plasmon resonance frequency and the width of the plasmon peak is known. For C_{60} the plasmon resonance frequency has been measured to be around 20 eV [79] and the width has been fitted to

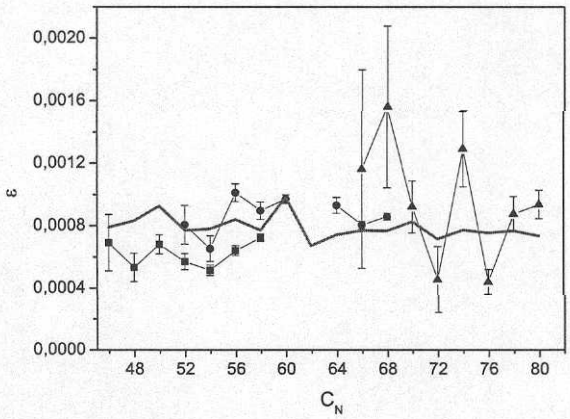

Figure 7.8: The thick solid line gives emissivities calculated using a single giant plasmon resonance and temperature $T = D/k_B G + D/2C_v$. The other symbols are the measured emissivities for ionic fragments of C_{60} (squares), C_{70} (circles) and C_{84} (triangles), the same as in Fig. 7.7.

15 eV [71]. Using these values in Eq. 7.16 and Eq. 7.17 and setting the temperature to $D/k_B G + D/2C_v$ as done before gives the thick solid line in Fig. 7.8. The main difference between the simple model described above and the one of Ref. [71] is that Andersen and Bonderup include a smaller plasmon resonance frequency around 6 eV [80]. This is probably the main reason for why the more simple model gives a consequently lower value than Andersen and Bonderup if one compares Fig. 7.7 and Fig. 7.8.

Laskin and Lifshitz have done the same kind of measurements of metastable fragmentation ratios as done here but they combined the time of flight mass spectrometer with a quadrupole ion trap [81]. The ion trap allows for cooling times up to 100 μs which means that the deviation of p from a straight line for small $\ln(t_2/t_1)$ could be observed (as mentioned in Appendix B). They included radiative cooling according to Ref. [72] and after a careful reanalysis (where consistency with previously measured breakdown curves [82] was required) results comparable to the present ones were obtained [83].

As discussed in Section 2.1 most measurements of radiative cooling of fullerenes require modeling of the competing decay channels. The previous inse-

curity regarding the value of the dissociation energy of C_{60} has thus led to the fact that many publications on radiative cooling are out of date. Another source of confusion has been the description of radiation from fullerenes using a black-body model. Quite often a black-body expression is used with a "Mie correction" for small particles, so that

$$I(\lambda, T) \propto \lambda^{-6} \frac{1}{e^{hc/(\lambda k_B T)} - 1}, \tag{7.18}$$

where I is the emission intensity, λ the wavelength of the emitted light and T the temperature. The "Mie correction" should compensate for the fact that the radiation is emitted by an object that is smaller than the typical wavelength of the light. However, in other cases the emission intensity is given as

$$I(\lambda, T) \propto \lambda^{-7} \frac{1}{e^{hc/(\lambda k_B T)} - 1}, \tag{7.19}$$

for example above and in Ref. [71]. The reason for the discrepancy between the two expressions (pointed out by e.g. Chupka and Klots [72]) stems from the correction for small particles due to Mie theory. In Refs. [71, 84] the absorption efficiency is given as

$$Q_{abs} = \frac{8\pi^2}{\lambda} r^3 Im\left[\frac{\epsilon - 1}{\epsilon + 2}\right] \tag{7.20}$$

where r is the radius of the (spherical) particle and ϵ is the dielectric function. If the dielectric function (or in other terms the polarizability) only weakly depends on the wavelength and can be considered constant the result in Eq. 7.18 is obtained. In other cases this is not valid (for example for metal particles as clearly stated on page 136 in Ref. [84]) and Eq. 7.19 should be used [71].

This makes a comparison of the present results with previously published data more troublesome. The modeling and results here also depend on the competing fragmentation since the dissociation energy D and the Gspann parameter G are needed. However, the table with the obtained values of $\varphi = \Delta(t_2 - t_1)$ in Paper III should allow for a reanalysis of the experiments in the future if needed.

7.4 Concluding remarks

Radiative cooling of gas phase fullerenes can be investigated via its influence on metastable fragmentation in a mass spectrometer. Emissivities of

fullerene ions C_{46}^{+} - C_{80}^{+} were estimated to lie between $5{\cdot}10^{-4}$ and $15{\cdot}10^{-4}$. However, some care needs to be taken since values for dissociation energies and the Gspann parameter have to be assumed. No major difference in the radiation behaviour between fullerenes and endohedral fullerenes was found. The radiation can be fairly well modeled by a free-electron description based on surface plasmons.

Chapter 8

Molecular fusion within clusters of C_{60}

The experiments on excitation of Rydberg states in C_{60} (Chapter 6) revealed some interesting features well worth to be investigated further. When clusters of fullerenes were excited by fs laser pulses they showed signs of C_2 fragmentation which was rather surprising (Section 6.2). To pursue the origin of this behaviour an experiment was set up in Göteborg.

8.1 Experimental

Clusters of fullerenes from the Cold Source were excited by laser pulses from a Clark femtosecond laser. The Cold Source was connected to the ReToF aligned directly on the axis of the Wiley-McLaren ion optics. Pure C_{60} was evaporated from an effusive oven and then the C_{60} vapour was cooled down to liq. N_2 temperatures as described in Chapter 3. At the oven temperature used, the C_{60} will aggregate creating clusters of fullerenes, $(C_{60})_N$. The experiments were also performed with C_{70}. The cluster distributions were checked by one photon ionising the clusters with the F_2 laser which was aligned parallel to the fs laser but coming from the other direction.

As initial experiments the C_{60} clusters from the Cold Source were excited by the fundamental of the fs laser (775 nm, ca. 200 fs in the interaction region, fluence 5-10 J/cm^2). They were then investigated in the ReTof where the reflectron was tuned for maximum mass resolution. The laser fluence was changed both by using neutral density filters and by changing the focusing of the laser beam. Different pressures of the He carrier/cooling gas in the Cold Source were also employed, leading to different cluster distributions.

8.2 Results and Discussion

A time of flight mass spectrum of $(C_{60})_N$ excited by femtosecond laser pulses looks quite different from spectra of the same species excited by other means, such as ion collisions or ns laser pulses. Fig. 8.1 shows a typical mass spectrum. The spectrum is dominated by the bimodal fragmentation pattern characteristic for C_{60} that has been excited by a powerful laser. At masses larger than C_{60} there are also groups of mass peaks where the peaks within the groups are separated by C_2 masses, similar to what is seen in Fig. 6.6. Surprisingly there are no pronounced peaks of $(C_{60})_2^+$, $(C_{60})_3^+$ and so on. The tail on the C_{60}^+ peak is not delayed ionisation but due to fragmentation of cluster ions to C_{60}^+ during the acceleration stage of the mass spectrometer. C_{60} mass spectra from the hot effusive source obtained under identical conditions does not show any tail on the C_{60}^+ peak. At the conditions used, the Cold Source does produce clusters of fullerenes, as discussed in Section 6.2 and in Refs. [40, 41]. The beam from the Cold Source contains $(C_{60})_N$ (see

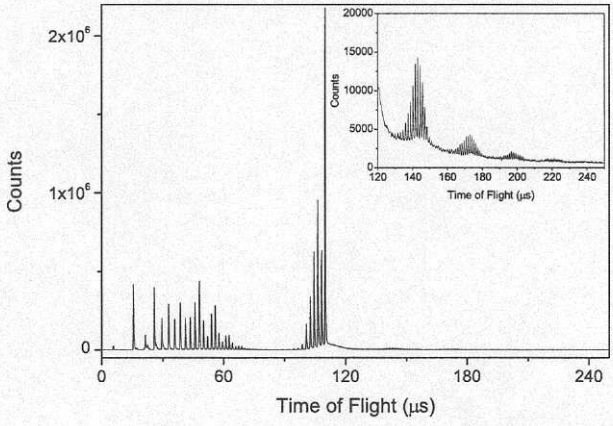

Figure 8.1: Time of flight mass spectrum of $(C_{60})_N$ clusters excited by fs laser pulses. The inset zooms in on the region where groups of fragments separated by C_2 masses appear.

Fig. 8.2 (c) and (d)) so to produce the fragment peaks in the groups, C_2 evaporation has to occur. C_2 evaporation from $(C_{60})_N$ is very unlikely. C_2 evaporation is characteristic for highly excited fullerenes but not for clusters

of fullerenes bound together by van der Waals forces. If, on the other hand, the $(C_{60})_N^+$ were to fuse to form a large fullerene-like molecule, C_2 evaporation would be expected if the internal energy is high enough.

Fig. 8.2 shows mass spectra obtained with the fs laser at two different Cold Source conditions together with the corresponding mass spectra obtained with the F_2 laser. Fig. 8.2 (a) and (c) correspond to a situation where the fullerene clusters grow very large (high carrier gas pressure). The maximum of the cluster distribution observed with the F_2 laser (8.2 (c)) seems to lie around $(C_{60})_{175}$ which the mass spectrometer can not resolve. When the fullerene clusters are smaller they can be nicely resolved by the spectrometer (Fig. 8.2 (d)) but the intensity of fragmented fused clusters is less (Fig. 8.2 (b)). There is generally a larger signal of fragments when the molecular beam contains large fullerene clusters. This could be because in large clusters a few fullerenes can boil off and there are still enough fullerenes in the cluster for fusion to take place.

Fusion/coalescence of fullerenes in the gas phase is a known phenomenon. Studies where C_{60} vapour was produced by laser desorption from a C_{60} film have shown evidence of fullerene coalescence under the right conditions [85–88]. The coalescence was dependent on the focusing conditions of the laser, a weak laser only gave C_{60}^+ in the mass spectra while a very focused laser gave an almost smooth distribution of C_{2n}^+ species from C_{60}^+ to more than C_{400}^+. At some intermediate laser focusing the distribution of C_{2n}^+ had symmetric maxima almost at C_{120}^+, C_{180}^+, C_{240}^+ and C_{300}^+. He gas was pulsed into the interaction region at the time of the laser pulse and the coalescence reaction was also dependent on the He pressure. It was concluded that the coalescence occurs in the gas phase rather than in the desorbed film. The fact that the fragment peak distribution is fairly symmetrical around C_{60N}^+ is due to the coalesced/coalescing species capturing C_2 molecules to form heavier objects[1]. This process requires a very dense vapour.

A similar fusion/coalescence behaviour must occur after fs excitation of $(C_{60})_N$ clusters in the gas phase. The clusters fuse to form fullerene like C_{60N} which then cool down by evaporating C_2 units. For fusion to occur a quite high density of fullerenes is required and also a quite high degree of excitation. The fs laser should supply enough excitation energy and the fullerene density is naturally high in the clusters. Fig. 8.3 shows the fragments of C_{120}^+, C_{180}^+, C_{240}^+ and C_{300}^+ in more detail. These spectra have been mass calibrated and a smooth background has been subtracted otherwise they are from the

[1] Actually, the distribution is symmetrical around C_{60N-2}^+.

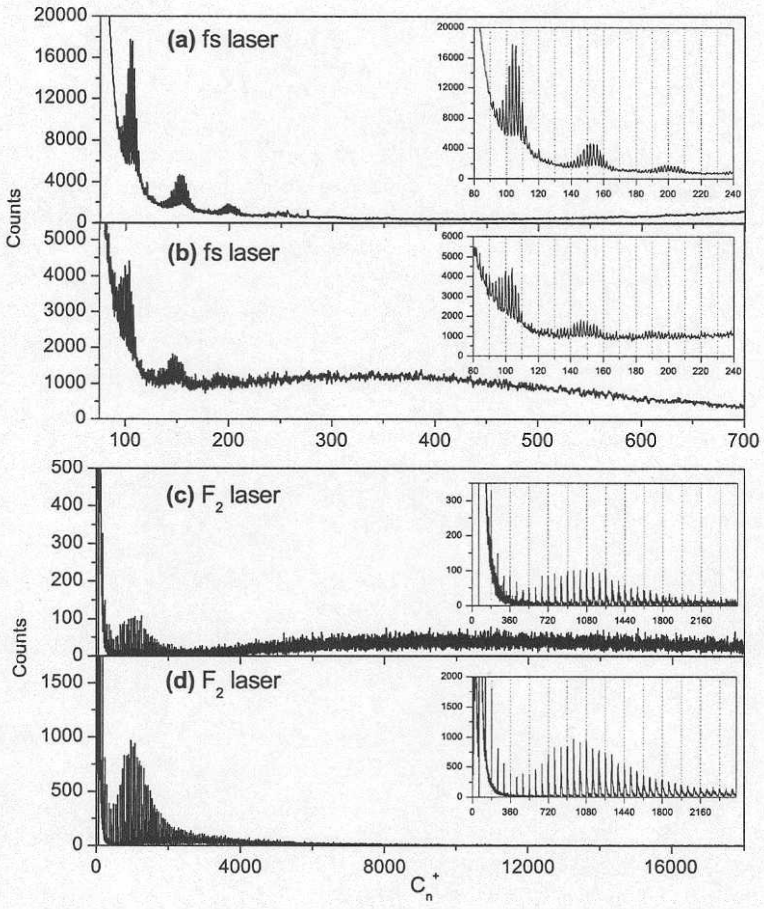

Figure 8.2: Mass spectra of fullerene clusters obtained under two different Cold Source conditions (**a** & **c**) and (**b** & **d**). **(a)** is obtained with a fs laser under the conditions where the fragmentation is easily visible (same conditions as in Fig. 8.1). The corresponding F_2 spectrum is shown in **(c)** where the fullerene clusters are very large, in the mass range the spectrometer can not resolve. In **(b)** and **(d)** the fullerene clusters are smaller and the fragments are less pronounced.

mass spectrum in Fig. 8.1. The distributions are rather narrow and they are

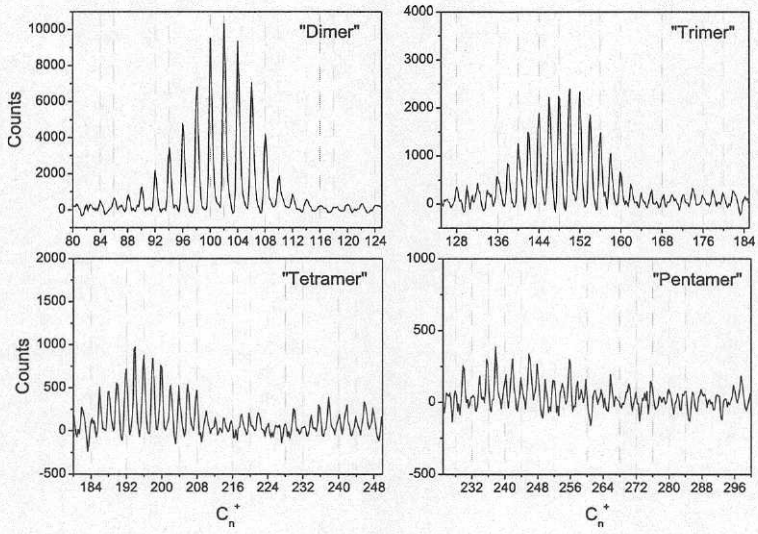

Figure 8.3: Fragmentation pattern of C_{120}^+, C_{180}^+, C_{240}^+ and C_{300}^+. The spectrum is the same as in Fig. 8.1 but it has been mass calibrated and a smooth background has been subtracted.

not observed to have picked up any C_2 molecules as in the laser desorption case. The latter is not surprising due to the over all low density of fullerene clusters in the beam (which means few C_2 to pick up). Regarding the narrow fragment distribution the upper limit of the distribution can be quite easily understood. Collision experiments where C_{60}^+ ions were collided with C_{60} have, together with theoretical studies, given a threshold energy for fusion of two C_{60} of 80-85 eV at 0 K [89–91]. This means that if the fullerenes have fused they must have an internal energy of at least 80 eV plus up to the heat of fusion which is ca 20 eV [92]. The amount of heat of fusion depends on the shape of the fused molecule. The initial shape in the present case is probably a peanut shape which has a heat of fusion $\sim$0 but this structure can later relax [92]. A fullerene with an internal energy of at least 85-105 eV will not stay intact for the time it takes for it to leave the acceleration stage of the mass spectrometer. It will instead cool down by emitting C_2 units giving rise

to the observed fragmentation pattern.

One can make some crude estimations and assume an Arrhenius pre-exponential factor for C_2 evaporation of $2{\cdot}10^{19}$ Hz and a dissociation energy of 8.5 eV, which seems to be a good average value for larger (positively charged) fullerenes. Considering the time it takes for the fullerenes to be mass separated in the spectrometer ($\sim$2.6 μs for C_{120}^+) and that they have at least 85 eV, as discussed above, it is possible to estimate that the heaviest fragment of C_{120} will be C_{116}^+. An internal energy of 105 eV will thus give rise to C_{112}^+. The most pronounced peak in the "dimer" group is C_{102}^+ (Fig. 8.3) which would correspond to an approximate internal energy of 135 eV. Assuming that all of the heat of fusion has been released and accounting for the ionisation energy this implies that the internal energy is $135 - 20 + 7.6 \approx 123$ eV just after photon absorption. That means $\sim$66 eV per C_{60} which, considering the fluence of 5-10 J/cm^2, is in fair agreement with the photoabsorption cross section estimated in Ref. [93]. Stretching the assumptions even further and saying that the maximum/centre of each fragment group comes from the clusters where each C_{60} absorbs 66 eV and all of the heat of fusion is released, gives maxima around C_{152}^+, C_{200}^+ and C_{248}^+. Comparing this to the actual maximum peaks in Fig. 8.3 shows that the estimated sizes are a little too large but considering the crude estimations, the agreement is quite good. From the mass spectra one can obtain the mean number of lost C_2 units from the dimer, trimer, tetramer and pentamer after integration over the mass peaks. The result is displayed in Fig. 8.4 together with the width of the fragment distributions.

The fragmentation pattern is similar when clusters of C_{70} are used. The mean number of lost C_2 units is a little bit larger as seen in Fig. 8.5 which is in agreement with the higher fusion barrier of 104 eV for C_{70} [91]. The same reasoning as above predicts that the maximum of the trimer fragments should be about C_{178}^+ which is a fair estimate but a little too high just as in the C_{60} case.

Changing the laser fluence gives a very small (if any) change in the fragment distribution as shown in Fig. 8.6. The almost constant widths of the fragment distributions are somewhat intriguing. One possible explanation is that a new decay channel becomes accessible with increasing internal energy. A good candidate for such a channel could be double ionisation.

Clusters of fullerenes have previously been studied after excitation by ion collisions. Highly charged, highly energetic Xe ions ($Xe^{20+,30+}$, 400$-$600 keV) were collided with $(C_{60/70})_N$ clusters and then examined in a high-resolution

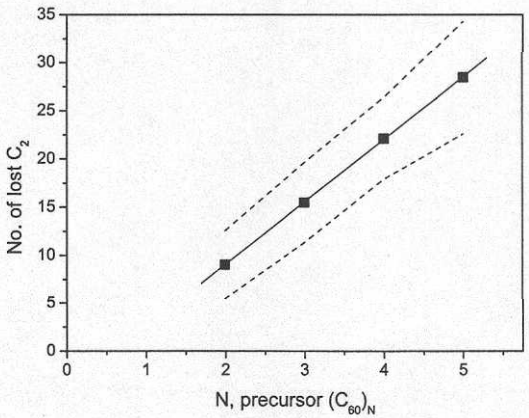

Figure 8.4: Number of lost C_2 units as a function of parent cluster size. The solid line is a linear fit to the data and the dashed lines represent the width of the fragment distributions.

ToF [94]. No C_2 evaporation except from C_{60}^+ was observed. Instead multiple ionisation occurred and clusters of fullerenes with charge up to 5+ and size $N = 33$ can be detected. The reason for the difference in fragmentation behaviour between the ion collisions and the above discussed ca. 200 fs laser excitation probably lies in different timescales. A Xe ion at 400 keV passes one fullerene diameter in ~1 fs which means that the interaction time is too short for the energy to couple to the electronic degrees of freedom, similar to the case with 25 fs laser pulses in Ref. [7].

8.3 Concluding remarks

Clusters of fullerenes have been shown to undergo C_2 evaporation after femtosecond laser excitation in the gas phase. The clusters undergo molecular fusion creating a more stable fullerene-like molecule. Fusion of C_{60} requires ca 85 eV per dimer and this energy, the heat of fusion plus any excess energy is then released from the molecule via C_2 evaporation. Further work is needed to investigate and explain the complete behaviour of the fragment distributions.

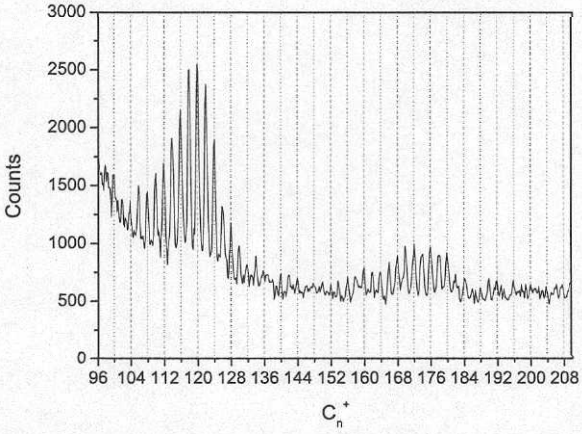

Figure 8.5: Fragmentation pattern obtained from fused $(C_{70})_N$ clusters, zoomed in on the region of fragments from C_{140}^+ and C_{210}^+.

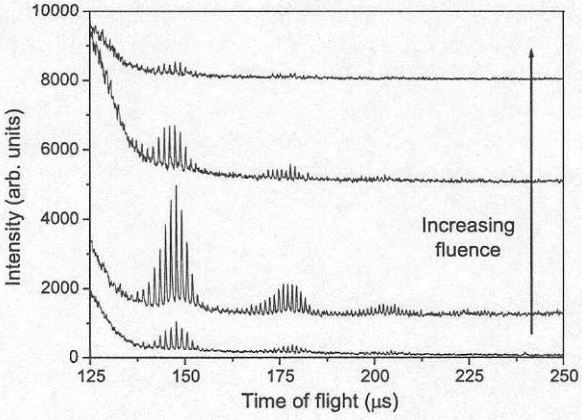

Figure 8.6: Time of flight mass spectra of $(C_{60})_N$ clusters after femtosecond laser irradiation with varying fluence. Almost no change at all is observed in the mass distribution.

Chapter 9

Conclusions and Outlook

In this work the behaviour of fullerenes and clusters of fullerenes after excitation by laser pulses has been investigated using mass spectrometric methods.

The lifetime of the lowest lying triplet state in C_{60} has been measured after laser excitation in the gas phase. The triplet state can be ruled out as being an important factor in the manifestation of delayed electron emission from C_{60}. The result is yet another indication that electron emission from fullerenes indeed is a completely statistical process. With the help of complementary work it can also be concluded that the triplet lifetime depends exponentially on the vibrational energy of the fullerene.

Other electronic states in C_{60} that have been investigated are the Rydberg states. The mechanisms behind the excitation of a quite broad range of Rydberg states using fs laser pulses are not completely understood. It was shown that the vibrational energy content of the C_{60} was of great importance. It was not possible to excite Rydberg states in vibrationally cold C_{60} by the same means used to routinely populate Rydberg states in hot (500 °C) fullerenes. Further investigations, both experimental and theoretical, are desirable to determine the precise process responsible for excitation of Rydberg states.

The two most prominent decay channels of highly excited fullerenes in the gas phase are ionisation and fragmentation. However, there is a third channel which is more anonymous and hard to measure directly, namely radiative cooling. Nevertheless a good understanding of radiative cooling is essential for a correct modeling of ionisation and fragmentation and for the analysis of many types of experimental data. The emissivity of laser excited fullerenes from C_{46}^+ to C_{82}^+ has been measured and in addition it was found that the

radiative behaviour was similar between endohedral fragments of $La@C_{82}^{+}$ and the corresponding fullerenes.

Clusters of fullerenes were discovered to show intriguing decay mechanisms when excited by femtosecond laser pulses. In a time of flight mass spectrometer they showed evidence of molecular fusion, from $(C_{60})_N$ to C_{60N}, followed by sequential C_2 evaporation. The behaviour is quite different compared to other means of excitation, like ion-impact or ns laser excitation, but can be understood by considering the short timescale and high power of the laser pulses.

The internal energy distribution of molecules after multiphoton absorption from a Gaussian laser beam was also examined. It was found that the internal energy distribution has a large low-energy part and that the distribution is proportional to a power law (up to a cutoff at a certain energy) which ranges from E^{-1} to $E^{-5/2}$ depending on the focusing of the laser. The Poisson distributions commonly used to describe internal energy distributions of laser excited molecules reproduce the high energy part at the cut off reasonably well but fail to describe the low energy part. This result is relevant not only for fullerene experiments but any spectroscopic measurements using laser excited molecular beams where low excitation energies can be important.

In summary this thesis has hopefully given, if not definite answers then at least some hints towards answers, to questions concerned with the understanding of large energetic molecules. It raises some new questions and points out some pitfalls to be avoided on the road towards a deeper understanding of our world.

The future

In the immediate future there are more experiments and modeling to be done to fully understand the dynamics of the fusion in fullerene clusters. On a longer timescale the future of fullerene and cluster experiments in Göteborg also looks quite interesting. The femtosecond laser system together with a ns OPO system and the other ns lasers provides the possibility to do a number of different pump-probe experiments. The mass spectrometer will also be equipped with a position sensitive photoelectron detector which will add one more dimension to the experiments. On my personal wish list would be a heating cell for the Cold Source so that one could produce fullerenes, or other clusters, with a specified temperature.

Regarding the future of the field the outcome of the experiments by Bordas and coworkers studying delayed ionisation at the Free Electron Laser for Infrared eXperiments (FELIX) will be interesting to follow. Preliminary results indicate that delayed electron emission from C_{60} excited by mid-IR photons is not thermal. Will the debate on the nature of delayed ionisation in C_{60} gain momentum once again?

Acknowledgements

Everyone who has contributed to this work in some way deserves appreciation. Klavs Hansen has been a never ending source of information, especially on messy statistical theories, approximations, series expansions, experimental techniques, criticism of my work, other peoples work and sometimes of his own work. His door has always been open for questions which I have deeply appreciated even though one often left with half an answer and several new problems to look into.

I am very grateful to my supervisor and examiner Eleanor Campbell for guiding me through these years. Not only has she shared her knowledge in physics and chemistry but also in some strange way always managed to find money when we needed to buy equipment. She has also not kept me locked up in the lab but allowed me to go to other laboratories and sent me to many conferences to present our work.

I would like to thank Alexander Bulgakov who has been a frequent visitor to our laboratory. He has taught me a lot about experimental work and his hard work has been an inspiration.

Andrei Gromov has supplied endless amounts of various types of fullerenes, chemicals and Spanish red wines. Mats Rostedt has helped with electronic issues, computer issues and almost any other practical issue. Heinrich Riedl has also been a source of information regarding chemicals and gases.

Thanks goes to Elin Rönnow and Fredrik Jonsson who did their diploma works on my project.

I very much enjoyed the weeks working at the Max Born Institute in Berlin together with Mark Boyle and Claus-Peter Schulz.

I am grateful to Christian Bordas, Franck Lépine and Francesca Pagliarulo for having me as a guest at Laboratoire de Spectrométrie Ionique et Moléculaire in Lyon.

I also thank Andreas Lassesson, Martin Sveningsson, Martin Jönsson and Mark Boyle not only for help in the lab but also for nice company outside of work.

I thank my office room mate Sergey Prasalovich (especially for all help on graphics), Mikael Kjellberg, Kirsten Mehlig, Frank Rohmund, Vladimir Popok and all other past and present members of the Atomic Physics group that have made this a pleasant place to work at.

A travel grant from Filosofiska fakulteternas gemensamma donationsnämnd is gratefully acknowledged.

Finally I have to thank my family and friends who have helped to keep me reasonably sane over the years.

Tack!

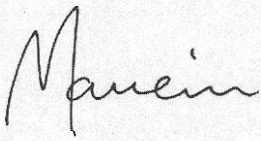

Appendices

Appendix A

Microcanonical temperature

Densities of states, or level densities, $\rho(E)$, are very important and commonly occurring in statistical theories describing clusters. In the canonical and grand canonical ensembles they can be used to determine the relation between energy and temperature. A similar connection can be derived for the microcanonical ensemble. The cluster dynamics dealt with here very often means taking a small part, ε, of the total cluster excitation energy, E, and depositing it in some degree of freedom like an evaporating atom or photon. The rest of the energy, $E-\varepsilon$, then has to be distributed among the remaining degrees of freedom giving a density of states within a certain energy interval like

$$\rho'(E-\varepsilon)d\varepsilon, \tag{A.1}$$

where the prime notes that there are a few degrees of freedom less than from the beginning. ε is assumed to be small enough to expand in. However, densities of states are quite strongly varying functions of energy, so rather than expanding the function directly in ε it is more correct to expand the logarithm of the function. Expanding the logarithm of $\rho'(E-\varepsilon)$ in ε gives

$$\ln(\rho'(E-\varepsilon)) = \ln(\rho'(E)) - \varepsilon\frac{d\ln(\rho'(E))}{dE} + \frac{\varepsilon^2}{2!}\frac{d^2\ln(\rho'(E))}{dE^2} - \frac{\varepsilon^3}{3!}\frac{d^3\ln(\rho'(E))}{dE^3} + \ldots \tag{A.2}$$

In analogy with canonical systems the second term in the expansion can be defined as ε/T where T is the temperature. Due to the fact that the system has a fixed energy T is not the normal temperature but is called the *microcanonical temperature*. When using the concept of microcanonical temperature care has to be taken not to use it for things it is not defined for. For large heat capacities the microcanonical temperature approaches the

canonical one (large meaning $C_v/k_B \gg 1$). The third term in the expansion is often called *the finite heat bath correction*. It can be rewritten like

$$\frac{\varepsilon^2}{2!}\frac{d^2\ln(\rho'(E))}{dE^2} = \frac{\varepsilon^2}{2!}\frac{d}{dE}\left(\frac{1}{T}\right) = \frac{\varepsilon^2}{2!}\left(-\frac{1}{T^2}\frac{dT}{dE}\right) = -\frac{\varepsilon^2}{2T^2}\frac{dT}{dE}. \tag{A.3}$$

Here it is possible to define the microcanonical heat capacity as $C_v = dE/dT$. The density of states for a system (e.g. cluster) with an initial excitation energy E where a small part ε has been deposited into a few specific degrees of freedom can then be given as

$$\rho'(E-\varepsilon) = \rho'(E)\exp\left(-\frac{\varepsilon}{T} - \frac{\varepsilon^2}{2}\frac{1}{C_v T^2} - \ldots\right). \tag{A.4}$$

This expression can be simplified further by recognising that $1/T + \varepsilon/(2C_vT^2)$ are the first two terms of the expansion of $(T - \varepsilon/(2C_v))$ in $\varepsilon/(2C_v)$ so that

$$\rho'(E-\varepsilon) \approx \rho'(E)\exp\left(-\frac{\varepsilon}{T-\frac{\varepsilon}{2C_v}}\right). \tag{A.5}$$

In a physical picture the exponential is the Boltzmann factor at the average temperature of the process, i.e. the mean of the temperature before and after the evaporation. In the case of evaporation of an atom from a cluster the energy ε will correspond to the dissociation energy (neglecting any kinetic energy of the evaporated atom). For photon emission from an excited cluster ε will be the photon energy, $h\nu$.

The description above was adapted from Ref. [74] which contains a rather comprehendible introduction to most concepts used to describe clusters by statistical theories.

Appendix B

Metastable fragmentation considering radiative cooling

Here follows the same derivation of the metastable fraction as done in Paper III but more explicit.

The decay of excited charged gas phase fullerenes (including radiative energy loss) is assumed to be described by a rate constant $k(t)$. If the logarithm of the rate constant is expanded in time one gets

$$ln(k(t)) = \ln(k(0)) + \frac{d\ln(k(t))}{dt} |_{t=0}\, t + ... \tag{B.1}$$

which in turn gives

$$k(t) = \exp[\ln(k(0)) + \frac{d\ln(k(t))}{dt} |_{t=0} + ...] \approx k(0)e^{-\varphi t}, \tag{B.2}$$

where φ is introduced as a parameter and will be discussed in detail below. It has been shown that it is easier to evaluate such expressions using micro-canonical temperatures rather than energies. Going from E to T renders

$$-\varphi = \frac{d\ln(k)}{dt} = \frac{d\ln(k)}{dT}\frac{dT}{dt} = \frac{d\ln(k)}{dT}\frac{-P(T_{Rad})}{C_v} \tag{B.3}$$

where $P(T_{Rad})$ is the power lost due to radiation as mentioned in Section 7.2 and C_v is the heat capacity. The further simplification of the expressions become easier if k is written in an Arrhenius form, $k = Ae^{-D/k_BT}$, (even

though this is strictly speaking not necessary):

$$-\varphi = \frac{d\ln(k)}{dT}\frac{-P(T_{Rad})}{C_v} = \frac{d}{dT}\left(\ln A - \frac{D}{k_B T}\right)\frac{-P(T_{Rad})}{C_v} = -\frac{D}{k_B T^2}\frac{P(T_{Rad})}{C_v}. \tag{B.4}$$

As also discussed in Section 7.2 the temperature T includes the finite heat bath (FHB) correction for dimer evaporation while the FHB correction is ignored for the radiative temperature T_{Rad}, partly for ease of calculation and partly for the reason that it is small. T_{Rad} can thus be expressed in terms of T like $T_{Rad} = T + D/(2C_v)$. By also (according to Stefan-Boltzmanns law) introducing $P = \varepsilon S \sigma_{SB} T_{Rad}^4$, where ε is the emissivity, σ_{SB} the Stefan-Boltzmann constant and S the surface area, and writing the temperature as $T \approx D/(Gk_B)$ (where G is the Gspann parameter) the final expression for the parameter φ becomes

$$\begin{aligned}\varphi = \frac{D}{k_B T^2}\frac{\varepsilon S \sigma_{SB}(T + D/(2C_v))^4}{C_v} &= \frac{D\varepsilon S\sigma_{SB}}{C_v k_B} T^2 \left(1 + \frac{D}{2C_v}\frac{1}{T}\right)^4 \approx \\ \approx \frac{D\varepsilon S\sigma_{SB}}{C_v k_B}\left(\frac{D}{Gk_B}\right)^2 \left(1 + \frac{DGk_B}{2C_v D}\right)^4 &= \frac{D^3 \varepsilon S \sigma_{SB}}{C_v G^2 k_B^3}\left(1 + \frac{Gk_B}{2C_v}\right)^4.\end{aligned} \tag{B.5}$$

Using Eq. B.5 one can compute the survival probability, $\rho(E,t)$, for a molecule starting with a specific energy at time $t = 0$, like

$$\begin{aligned}&\frac{d\rho(E)}{dt} = -k(E,t)\rho(E) = -k(E,0)e^{-\varphi t}\rho(E) \Rightarrow \\ &\Rightarrow \frac{1}{\rho(E)}\frac{d\rho(E)}{dt} = \frac{d\ln(\rho(E))}{dt} = -k(E,0)e^{-\varphi t}.\end{aligned} \tag{B.6}$$

Integrating the logarithm of the survival probability gives

$$\begin{aligned}&\int_0^t d\ln(\rho(E)) = \ln(\rho(E,t)) - \ln(\rho(E,0)) = \\ &= \int_0^t -k(E,0)e^{-\varphi t}dt = \frac{k(E,0)}{\varphi}(e^{-\varphi t} - 1)\end{aligned} \tag{B.7}$$

and to obtain $\rho(E,t)$ take the exponential of Eq. B.7 like

$$\begin{aligned}\exp(\ln(\rho(E,t)) - \ln(\rho(E,0))) = \frac{\rho(E,t)}{\rho(E,0)} &= \exp\left(-\frac{k(E,0)}{\varphi}(1 - e^{-\varphi t})\right) \Rightarrow \\ \Rightarrow \rho(E,t) &= \rho(E,0)e^{-\frac{k(E,0)}{\varphi}(1-e^{-\varphi t})}.\end{aligned} \tag{B.8}$$

Eq. B.8 gives an expression for the survival probability for a molecule at the time t. For a certain fragment size N there is a high energy cutoff in the internal energy distribution as discussed in Section 7.2 which is given by

$$f_+(E,t) = e^{-\frac{k_N(E,0)}{\varphi_N}(1-e^{-\varphi_N t})}. \tag{B.9}$$

The high energy cutoff for the precursor molecule $N+2$ gives the low energy cutoff for N,

$$f_-(E,t) = 1 - e^{-\frac{k_{N+2}(E+D,0)}{\varphi_{N+2}}(1-e^{-\varphi_{N+2} t})}. \tag{B.10}$$

The energy distribution is then given by putting f_+ and f_- together with $\rho(E,0)$ like

$$f(E,t) = \rho(E,0) f_+ f_- = \rho(E,0) e^{-\frac{k_N(E,0)}{\varphi_N}(1-e^{-\varphi_N t})}\left(1-e^{-\frac{k_{N+2}(E+D,0)}{\varphi_{N+2}}(1-e^{-\varphi_{N+2} t})}\right). \tag{B.11}$$

f is the energy distribution for non size selected fragments. When size selection has been realised in the mass spectrometer ($t > t_1$) the lower cutoff will not move (except for a small change due to radiative energy loss) while the higher cutoff will keep moving until the ion fragments reach the reflectron at time t_2. The calculated distributions for C_{50}^+ at time t_1 and t_2 are shown in Fig. B.1. The area between the solid and the dashed line corresponds to the the part of the molecules that undergo metastable fragmentation. Assuming that f_- and f_+ are well separated and that the area of the distribution can be considered proportional to the width one can relate the motion of the high energy cutoff to the metastable fragmentation rate. The specific cutoff energy E_c is defined as the point where f_+ has its maximum slope which is determined by

$$\frac{d^2}{dE^2}\left(e^{\frac{k(E_c,0)}{\varphi}(1-e^{-\varphi t})}\right) = 0 \Rightarrow \frac{k(E_c,0)}{\varphi}(1-e^{-\varphi t}) = 1. \tag{B.12}$$

An expression for the cutoff energy E_c can be obtained by writing the decay rate in an Arrhenius form, $k_N = Ae^{-D_N/k_B T(E)}$, and using the caloric curve $E = C_v T + E'$ which turns Eq. B.12 into

$$\begin{aligned}
&\frac{k(E_c,0)}{\varphi_N}(1-e^{-\varphi_N t}) = 1 = \frac{Ae^{-D_N/k_B T(E_c)}}{\varphi_N}(1-e^{-\varphi_N t}) \Leftrightarrow \\
&\Leftrightarrow \ln\left(\frac{\varphi_N}{A(1-e^{-\varphi_N t})}\right) = -\frac{D_N}{k_B T(E_c)} = -\frac{C_v D_N}{k_B(E_c - E')} \Rightarrow \\
&\Rightarrow E_c = \frac{C_v D_N}{k_B \ln\left(\frac{A}{\varphi_N}(1-e^{-\varphi_N t})\right)} + E'.
\end{aligned} \tag{B.13}$$

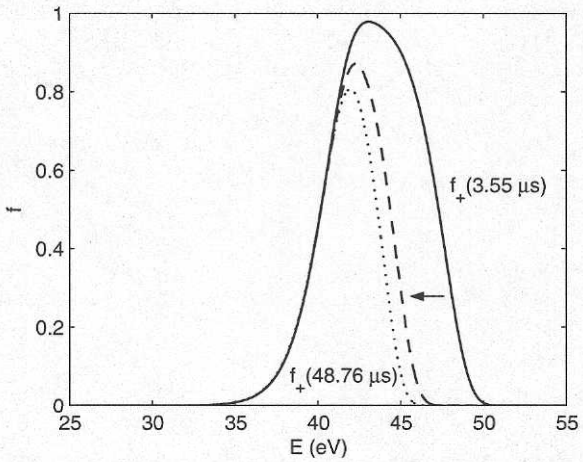

Figure B.1: Calculated internal energy distributions for C_{50}^{+} at time $t_1 = 3.55$ μs (solid line) and at $t_2 = 48.76$ μs (dashed line). The dotted line shows the energy distribution at t_2 if radiative cooling is neglected (same situation as in Fig. 7.1). The dissociation energy is set to 8.8 eV, $A = 2{\cdot}10^{19}$ Hz, $E_0 = 7.04$ eV and the emissivity $\varepsilon = 0.0007$.

The metastable fraction is

$$p \propto \int_{E_c(t_2)}^{E_c(t_1)} \rho(E) dE. \tag{B.14}$$

If $\rho(E,0)$ can be considered constant[1] then

$$p \propto \frac{1}{D_N} \frac{C_v D_N}{\ln\left(\frac{A}{\varphi_N}(1-e^{-\varphi_N t_1})\right)} - \frac{C_v D_N}{\ln\left(\frac{A}{\varphi_N}(1-e^{-\varphi_N t_2})\right)}, \tag{B.15}$$

where the factor $1/D_N$ accounts for the width of the distribution. Changing variables $r \equiv t_1/t_2$ and $\Delta \equiv \varphi_N(t_2 - t_1)$ (or in other words $t_2 \equiv \Delta/(\varphi(1-r))$ and $t_1 \equiv \Delta r/(\varphi(1-r))$) allows for an expansion in r if φt_1 can be considered small. φt_1 is small if the radiative cooling is small on the timescale of t_1 which should be a justified assumption. Eq. B.15 becomes

$$p \propto C_v \frac{k_B \ln\left(\frac{1-e^{-\Delta/(1-r)}}{1-e^{-\Delta r/(1-r)}}\right)}{\ln\left(\frac{A}{\varphi_N}(1-e^{-\Delta/(1-r)})\right) \ln\left(\frac{A}{\varphi_N}(1-e^{-\Delta r/(1-r)})\right)}. \tag{B.16}$$

[1]This assumption is released in Paper III.

Expanding the exponentials around 0 gives

$$e^{-\frac{\Delta}{1-r}} = e^{-\Delta} + \frac{-\Delta}{(1-r)^2} e^{-\frac{\Delta}{1-r}} \mid_{r=0} r + ... = e^{-\Delta} - \Delta r e^{-\Delta} + ... \quad \text{(B.17)}$$

and

$$e^{-\frac{\Delta r}{1-r}} = 1 - \Delta \left(\frac{1}{1-r} + \frac{r}{(1-r)^2} \right) e^{-\frac{\Delta r}{1-r}} \mid_{r=0} r + ... = 1 - \Delta r + ... \quad \text{(B.18)}$$

which renders

$$\ln \left(\frac{1 - e^{-\frac{\Delta}{1-r}}}{1 - e^{-\frac{\Delta r}{1-r}}} \right) = \ln \left(\frac{1 - e^{-\Delta} + \Delta r e^{-\Delta} + ...}{1 - 1 + \Delta r + ...} \right) =$$

$$= \ln \left(\frac{(1 - e^{-\Delta})(1 + \frac{\Delta r e^{-\Delta})}{1 - e^{-\Delta}} + ...)}{\Delta r + ...} \right) \approx \ln \left(\frac{1 - e^{-\Delta}}{\Delta} \right) + \ln \left(\frac{1}{r} \right). \quad \text{(B.19)}$$

The factors in the denominator becomes

$$\ln \left(\frac{A}{\varphi_N} (1 - e^{-\frac{\Delta}{1-r}}) \right) \approx \ln \left(\frac{A}{\varphi_N} (1 - e^{-\Delta}) \right) = \ln \left(\frac{A}{\varphi_N} (1 - e^{-\varphi_N (t_2 - t_1)}) \right) \equiv G', \quad \text{(B.20)}$$

and

$$\ln \left(\frac{A}{\varphi_N} (1 - e^{-\frac{\Delta r}{1-r}}) \right) \approx \ln \left(\frac{A}{\varphi_N} (1 - (1 - \Delta r)) \right) = \ln \left(\frac{A}{\varphi_N} \Delta r \right) =$$

$$= \ln \left(\frac{A}{\varphi_N} \varphi_N (t_2 - t_1) \frac{t_1}{t_2} \right) \approx \ln(A t_1) \equiv G. \quad \text{(B.21)}$$

Collecting everything and inserting into Eq. B.16 gives an expression for the metastable fragmentation ratio

$$p \propto \frac{C_v}{k_B G G'} \left(\ln(t_2/t_1) + \ln \left(\frac{1 - e^{-\Delta}}{\Delta} \right) + O(r) \right). \quad \text{(B.22)}$$

The metastable fragmentation ratio for C_{50}^+ calculated numerically using the "full" expression of Eq. B.11 is plotted in Fig. B.2 for a large span of $\ln(t_2/t_1)$. The circles mark where the experimental data points are collected. The straight line is calculated by the approximate expression for the metastable fragmentation ratio, p, Eq. B.22. The "full" calculation reproduces the deviation from a straight line at small and large values of $\ln(t_2/t_1)$ as also seen

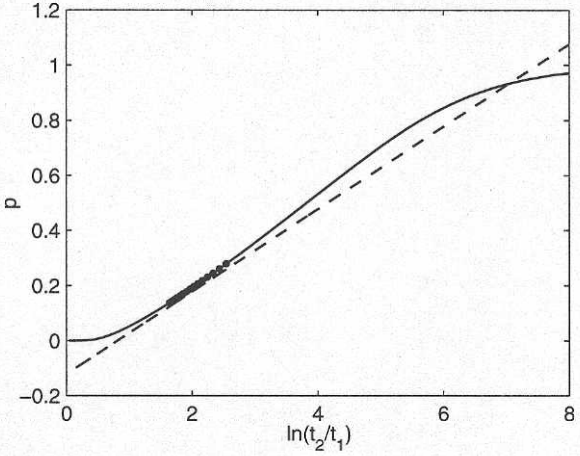

Figure B.2: Metastable fragmentation ratios calculated for C_{50}^{+} using the "full" expression, Eq. B.11, (solid line) and the approximation, Eq. B.22 (dashed line). The circles mark the times where the experimental measurements are done.

experimentally by Laskin and Lifshitz [81]. Even in the region of the present experiments, where both curves are more or less straight lines, there is a slight difference. The error this gives rise to in the analysis of the experiments was estimated by calculating p at the values of $\ln(t_2/t_1)$ where the experiments were done using both the "full" expression and the approximation and then fitting straight lines to these values. From the fitted lines values of the parameter φ (which is proportional to the emissivity) could be calculated. In general the approximation gave a value 7-8% higher than the full calculation.

Bibliography

[1] H. W. Kroto, J. R. Heath, S. C. O'Brien, R. F. Curl, and R. E. Smalley, *Nature*, **318**, 162 (1985).

[2] L. V. Radushkevich and V. M. Luk'yanovich, *Zhurnal Fizicheskoi Khimii*, **26**, 88 (1952).

[3] S. Iijima, *Nature*, **354**, 56 (1991).

[4] W. Krätschmer, L. D. Lamb, K. Fostiropoulos, and D. R. Huffmann, *Nature*, **347**, 354 (1990).

[5] J. de Vries, H. Steger, B. Kamke, C. Menzel, B. Weisser, W. Kamke, and I. V. Hertel, *Chem. Phys. Lett.*, **188**, 159 (1992).

[6] V. J. Bhardwaj, P. B. Corkum, and D. M. Rayner, *Phys. Rev. Lett.*, **91**, 203004 (2003).

[7] E. E. B. Campbell, K. Hansen, K. Hoffmann, G. Korn, M. Tchaplyguine, M. Wittman, and I. V. Hertel, *Phys. Rev. Lett.*, **84**, 2128 (2000).

[8] S. Tomita, J. U. Andersen, K. Hansen, and P. Hvelplund, *Chem. Phys. Lett.*, **382**, 120 (2003).

[9] E. E. B. Campbell, G. Ulmer, and I. V. Hertel, *Phys. Rev. Lett.*, **67**, 1986 (1991).

[10] G. C. Nieman, E. K. Parks, S. C. Richtsmeier, K. Liu, L. G. Probo, and et al., *High. Temp. Sci.*, **22**, 115 (1986).

[11] E. E. B. Campbell and R. D. Levine, *Annu. Rev. Phys. Chem.*, **51**, 65 (2000).

[12] J. U. Andersen, E. Bonderup, and K. Hansen, *J. Phys. B*, **35**(5), R1–R30 (2002).

[13] M. Boyle, K. Hoffmann, C. P. Schulz, I. V. Hertel, R. D. Levine, and E. E. B. Campbell, *Phys. Rev. Lett.*, **87**, 273401 (2001).

[14] C. Lifshitz, *Int. J. Mass Spectrom.*, **200**, 423 (2000).

[15] D. Muigg, P. Scheier, and T. D. Märk, *J. Phys. B*, **29**, 5193 (1996).

[16] G. von Helden, M. T. Hsu, P. R. Kemper, and M. T. Bowers, *J. Chem. Phys.*, **95**, 3835 (1991).

[17] S. Matt, O. Echt, M. Sonderegger, R. David, P. Scheier, J. Laskin, C. Lifshitz, and T. D. Märk, *Chem. Phys. Lett.*, **303**, 379 (1999).

[18] P. Sandler, C. Lifshitz, and C. Klots, *Chem. Phys. Lett.*, **200**, 445 (1992).

[19] E. E. B. Campbell, *Fullerene Collision Reactions*, Kluwer Academic Publishers, 2003.

[20] C. Lifshitz, *Int. J. Mass Spectrom.*, **198**, 1 (2000).

[21] S. Díaz-Tendero, M. Alcamí, and F. Martín, *J. Chem. Phys.*, **119**, 5545 (2003).

[22] K. Gluch, S. Matt-Leubner, O. Echt, B. Concina, P. Scheier, and T. Märk, *J. Chem. Phys.*, **121**, 2137 (2004).

[23] B. Concina, S. Tomita, J. U. Andersen, and P. Hvelplund, *Eur. Phys. J. D, in press* (2005).

[24] K. Hansen and E. E. B. Campbell, *J. Chem. Phys.*, **104**, 5012 (1996).

[25] J. Gspann In S. Datz, Ed., *Physics of electronic and atomic collisions*, 1982.

[26] R. Mitzner and E. E. B. Campbell, *J. Chem. Phys.*, **103**, 2445 (1995).

[27] A. A. Vostrikov, A. A. Agarkov, and D. Y. Dubov, *Tech. Phys.*, **45**, 915 (2000).

[28] J. R. Heath, S. C. O'Brien, Q. Zhang, Y. Liu, R. F. Curl, H. W. Kroto, F. K. Tittel, and R. E. Smalley, *J. Am. Chem. Soc.*, **107**, 7780 (1985).

[29] H. Shinohara, *Rep. Prog. Phys.*, **63**, 843 (2000).

[30] R. Tellgmann, N. Krawez, S.-H. Lin, I. V. Hertel, and E. E. B. Campbell, *Nature*, **382**, 407 (1996).

[31] E. E. B. Campbell, R. Tellgmann, N. Krawez, and I. V. Hertel, *J. Phys. Chem. Solids*, **58**, 1763 (1997).

[32] A. Gromov, W. Krätschmer, N. Krawez, R. Tellgmann, and E. E. B. Campbell, *Chem. Commun.*, page 2003 (1997).

[33] A. Lassesson *Fullerenes with Confined Atoms - The structure and dynamics of* $Li@C_{60}$ *and* $La@C_{82}$ PhD thesis, Göteborg University/Chalmers University of Technology, (2003).

[34] M. Jönsson, *Structure and Oxygen Sensitivity of Endohedral Fullerenes*, Licenciate Thesis, Göteborg University, (2005).

[35] W. C. Wiley and I. H. McLaren, *Rev. Sci. Instrum.*, **26**, 1150 (1955).

[36] V. I. Karataev, B. A. Mamyrin, and D. V. Shmikk, *Sov. Phys.-Tech. Phys.*, **16**, 1177 (1972).

[37] B. A. Mamyrin, V. I. Karataev, and V. A. Zagulin, *Sov. Phys.-JETP*, **37**, 45 (1973).

[38] D. R. Miller, *Atomic and Molecular Beam Methods*, Vol. 1, Oxford University Press, 1988.

[39] T. P. Martin, U. Näher, H. Schaber, and U. Zimmermann, *Phys. Rev. Lett.*, **70**, 3079 (1993).

[40] K. Hansen, R. Müller, H. Hohmann, and E. E. B. Campbell, *Z. Phys. D*, **40**, 361 (1997).

[41] K. Hansen, H. Hohmann, R. Müller, and E. E. B. Campbell, *J. Chem. Phys.*, **105**, 6088 (1996).

[42] A. V. Bulgakov, O. F. Bobrenok, V. I. Kosyakov, I. Ozerov, W. Marine, M. Hedén, F. Rohmund, and E. E. B. Campbell, *Phys. Solid State*, **44**, 594 (2002).

[43] G. von Helden, I. Holleman, A. J. A. van Roij, G. M. H. Knippels, A. F. G. van der Meer, and G. Meijer, *Phys. Rev. Lett.*, **81**, 1825 (1998).

[44] K. Hansen and O. Echt, *Phys. Rev. Lett.*, **78**, 2337 (1997).

[45] F. Rohmund, M. Hedén, A. V. Bulgakov, and E. E. B. Campbell, *J. Chem. Phys.*, **115**, 3068 (2001).

[46] R. E. Haufler, L.-S. Wang, L. P. F. Chibante, C. Jin, J. Conceicao, Y. Chai, and R. E. Smalley, *Chem. Phys. Lett.*, **179**, 449 (1991).

[47] H. T. Etheridge III, R. D. Averitt, N. J. Halas, and R. B. Weisman, *J. Phys. Chem.*, **99**, 11306 (1995).

[48] M. R. Fraelich and R. B. Weisman, *J. Phys. Chem.*, **97**, 11145 (1993).

[49] M. R. Wasielewski, M. P. O'Neil, K. R. Lykke, M. J. Pellin, and D. M. Gruen, *J. Am. Chem. Soc.*, **113**, 2774 (1991).

[50] D. J. van den Heuvel, I. Y. Chan, E. J. J. Groenen, J. Schmidt, and G. Meijer, *Chem. Phys. Lett.*, **231**, 111 (1994).

[51] P. Wurz and K. R. Lykke, *Chem. Phys.*, **184**, 335 (1994).

[52] D. Ding, R. N. Compton, R. E. Haufler, and C. E. Klots, *J. Phys. Chem.*, **97**, 2500 (1993).

[53] Y. Zhang and M. Stuke, *Phys. Rev. Lett.*, **70**, 3231 (1993).

[54] M. S. Dresselhaus, G. Dresselhaus, and P. C. Eklund, *Science of Fullerenes and Carbon Nanotubes*, Academic Press, 1996.

[55] R. Deng, M. Treat, O. Echt, and K. Hansen, *J. Chem. Phys.*, **118**, 8563 (2003).

[56] O. Echt, S. Yao, R. Deng, and K. Hansen, *J. Phys. Chem.*, **108**, 6944 (2004).

[57] D. M. Guldi and P. Kamat, *Fullerenes: Chemistry, Physics and Technology*, John Wiley & Sons: New York, 2000.

[58] C. Bordas, B. Baguenard, B. Climen, M. A. Lebeault, F. Lépine, and F. Pagliarulo *Eur. Phys. J. D, in press*, (2004).

[59] K. Hansen, J. U. Andersen, P. Hvelplund, S. P. Møller, U. V. Pedersen, and V. V. Petrunin, *Phys. Rev. Lett.*, **87**, 123401 (2001).

[60] P. Stampfli and T. D. Märk, *Phys. Rev. Lett.*, **82**, 459 (1999).

[61] S. Tomita, J. U. Andersen, C. Gottrup, P. Hvelplund, and U. V. Pedersen, *Phys. Rev. Lett.*, **87**, 073401 (2001).

[62] M. Foltin, M. Lezius, P. Scheier, and T. D. Märk, *J. Chem. Phys.*, **98**, 9624 (1993).

[63] J. Berkowitz, *Atomic and Molecular Photoabsorption: Absolute Total Cross Sections*, Academic, San Diego, 2002.

[64] F. Remacle and R. D. Levine, *Int. J. Quantum Chem.*, **67**, 85 (1998).

[65] C. P. Schick and P. M. Weber, *J. Phys. Chem*, **105**, 3735 (2001).

[66] M. Tchaplyguine, K. Hoffmann, O. Dühr, H. Hohmann, G. Korn, H. Rottke, M. Wittmann, I. V. Hertel, and E. E. B. Campbell, *J. Chem. Phys.*, **112**, 2781 (2000).

[67] M. Boyle, M. Hedén, C. P. Schulz, E. E. B. Campbell, and I. V. Hertel, *Phys. Rev. A*, **70**, 051201 (2004).

[68] M. Boyle, T. Laarmann, K. Hoffmann, M. Hedén, C. P. Schulz, E. E. B. Campbell, and I. V. Hertel, *Submitted to Eur. Phys. J. D.*

[69] G. P. Zhang, X. Sun, and T. F. George, *Phys. Rev. B*, **68**, 165410 (2003).

[70] W. Branz, N. Malinowski, H. Schaber, and T. P. Martin, *Chem. Phys. Lett.*, **328**, 245 (2000).

[71] J. U. Andersen and E. Bonderup, *Eur. Phys. J. D*, **11**, 413 (2000).

[72] W. A. Chupka and C. E. Klots, *Int. J. Mass Spectrom. Ion Proc.*, **167/168**, 595 (1997).

[73] J. Lemaire, M. Heninger, R. Marx, and G. Mauclaire, *Int. J. Mass Spectrom.*, **189**, 93 (1999).

[74] K. Hansen, *Statistical Physics of Nanoparticles.*, 2003.

[75] K. Hansen and U. Näher, *Phys. Rev. A*, **60**, 1240 (1999).

[76] T. Peres, B. Cao, H. Shinohara, and C. Lifshitz, *Int. J. Mass Spectrom.*, **228**, 181 (2003).

[77] K. Hansen and L. Schweikhard, Elsevier, Amsterdam, Boston, 2003; chapter Metal Clusters.

[78] W. A. de Heer, *Rev. Mod. Phys.*, **65**(3), 611–676 (1993).

[79] I. V. Hertel, H. Steger, J. de Vries, B. Weissner, C. Menzel, B. Kamke, and W. Kamke, *Phys. Rev. Lett.*, **68**, 784 (1992).

[80] D. Östling, P. Apell, and A. Rosén, *Z. Phys. D*, **26**, 282 (1993).

[81] J. Laskin and C. Lifshitz, *Chem. Phys. Lett.*, **277**, 564 (1997).

[82] R. Wörgötter, B. Dünser, T. D. Märk, M. Foltin, C. E. Klots, J. Laskin, and C. Lifshitz, *J. Chem. Phys.*, **104**, 1225 (1996).

[83] J. Laskin, B. Hadas, T. D. Märk, and C. Lifshitz, *Int J. Mass Spectrom.*, **177**, L9 (1998).

[84] C. E. Bohren and D. R. Huffman, *Absorption and Scattering of Light by Small Particles*, John Wiley, New York, 1983.

[85] C. Yeretzian, K. Hansen, F. Diedrich, and R. L. Whetten, *Nature*, **359**, 44 (1992).

[86] C. Yeretzian, K. Hansen, F. Diedrich, and R. L. Whetten, *Z. Phys. D*, **26**, 300 (1993).

[87] R. D. Beck, P. Weis, G. Bräuchle, and M. M. Kappes, *J. Chem. Phys.*, **100**, 262 (1993).

[88] R. Mitzner, B. Winter, C. Kusch, E. E. B. Campbell, and I. V. Hertel, *Z. Phys. D*, **37**, 89 (1996).

[89] F. Rohmund, E. E. B. Campbell, O. Knospe, G. Seifert, and R. Schmidt, *Phys. Rev. Lett.*, **76**, 3289 (1996).

[90] F. Rohmund, A. Glotov, K. Hansen, and E. E. B. Campbell, *J. Phys. B: At. Mol. Opt. Phys.*, **29**, 5143 (1996).

[91] O. Knospe, A. Glotov, G. Seifert, and R. Schmidt, *J. Phys. B: At. Mol. Opt. Phys.*, **29**, 5163 (1996).

[92] D. L. Strout, R. L. Murry, C. Xu, W. C. Eckhoff, G. K. Odom, and G. E. Scuseria, *Chem. Phys. Lett.*, **214**, 576 (1993).

[93] K. Hansen, K. Hoffmann, and E. E. B. Campbell, *J. Chem. Phys.*, **119**, 2513 (2003).

[94] B. Manil, L. Maunoury, B. A. Huber, J. Jensen, H. T. Schmidt, H. Zettergren, H. Cederquist, S. Tomita, and P. Hvelplund, *Phys. Rev. Lett.*, **91**, 215504 (2003).

GÖTEBORGS UNIVERSITET
GÖTEBORGS UNIVERSITETSBIBLIOTEK

GÖTEBORG
UNIVERSITY

Faculty of Science

ISBN 91-628-6541-2